AD_____

Award Number: DAMD17-01-2-0047

TITLE: Disaster Relief and Emergency Medical Services Project (DREAMS TM): Science, Triage, and Treatment (STAT)

PRINCIPAL INVESTIGATOR: Samuel W. Casscells, M.D.

CONTRACTING ORGANIZATION: The University of Texas Health Sciences Center at Houston
Houston, Texas 77030-3900

REPORT DATE: October 2003

TYPE OF REPORT: Annual

PREPARED FOR: U.S. Army Medical Research and Materiel Command
Fort Detrick, Maryland 21702-5012

DISTRIBUTION STATEMENT: Approved for Public Release;
Distribution Unlimited

REPORT DOCUMENTATION PAGE

Form Approved
OMB No. 074-0188

1. AGENCY USE ONLY (Leave blank)	2. REPORT DATE	3. REPORT TYPE AND DATES COVERED
	October 2003	Annual (15 Sep 2002 - 15 Sep 2003)

4. TITLE AND SUBTITLE
Disaster Relief and Emergency Medical Services Project (DREAMS TM): Science, Triage, and Treatment (STAT)

5. FUNDING NUMBERS
DAMD17-01-2-0047

6. AUTHOR(S)
Samuel W. Casscells, M.D.

7. PERFORMING ORGANIZATION NAME(S) AND ADDRESS(ES)
The University of Texas Health Sciences Center at Houston
Houston, Texas 77030-3900

E-Mail: s.ward.casscells@uth.tmc.edu

8. PERFORMING ORGANIZATION REPORT NUMBER

9. SPONSORING / MONITORING AGENCY NAME(S) AND ADDRESS(ES)
U.S. Army Medical Research and Materiel Command
Fort Detrick, Maryland 21702-5012

10. SPONSORING / MONITORING AGENCY REPORT NUMBER

11. SUPPLEMENTARY NOTES
Original contains color plates: All DTIC reproductions will be in black and white.

12a. DISTRIBUTION / AVAILABILITY STATEMENT
Approved for Public Release; Distribution Unlimited

12b. DISTRIBUTION CODE

13. ABSTRACT (Maximum 200 Words)
Science, Triage, and Treatment is the component of DREAMS (Disaster Relief and Emergency Medical Services) that is developing new ways to diagnose and treat tissue injuries and infection. Progress has been the pathophysiology and molecular biology of anthrax, human cytochrome P450 defenses, inflammation, oxidation, apoptosis, reperfusion injury, organ failure, and nitric oxide. New techniques have been developed to automatically diagnose ischemia and heart, kidney, and respiratory failure. STAT scientists have also developed new techniques to diagnose and image tissue inflammation and necrosis using CT, magnetic resonance, thermal imaging, and near-infrared spectroscopy. These have led to numerous publications, patents, products, clinical trials, and awards. In addition to trauma and infection, likely application include atherosclerosis and cancer. In summary, DREAMS-STAT is making better than expected progress toward its goal of improving the care of battlefield injuries.

14. SUBJECT TERMS
No Subject Terms Provided.

15. NUMBER OF PAGES
63

16. PRICE CODE

17. SECURITY CLASSIFICATION OF REPORT	18. SECURITY CLASSIFICATION OF THIS PAGE	19. SECURITY CLASSIFICATION OF ABSTRACT	20. LIMITATION OF ABSTRACT
Unclassified	Unclassified	Unclassified	Unlimited

Table of Contents

1. Cover Sheet..... 1

2. Standard Form 298..... 2

3. Table of Contents..... 3

4. Project I.A..... 5

Administrative Section (Willerson, Casscells)

5. Project I.B..... 7

Mechanisms of Cardiomyocyte Injury in Shock (Buja)

6. Project I.C.1..... 15

Molecular Regulation of Apoptosis in Wound Healing (Geng)

7. Project I.C.2..... 18

Infrared Spectroscopic Diagnosis of Vulnerable Atherosclerotic Plaque (Casscells)

8. Project I.C.4..... 22

Nitric Oxide in Organ Failure (Kone)

9. Project I.C.6..... 27

Is Hypothermia an Indicator of Imminent Death in Congestive Heart Failure and Helpful in Triage (Casscells)

10. Project I.D..... 30

Up-regulation of P450: A Natural, Broad-Based Defense Against Chemical and Biological Threats (Strobel)

11. Project I.E..... 32

Detection and Quantitation of Bacillus anthracis in Macrophages (Koehler)

12. Project II.A..... 36

Pathology Core (Willerson, Buja, Litovsky)

13. Project II.D..... 37

Thermal Detection and Treatment of Inflammation and Necrosis (Casscells)

14. Project 1I.E..... 40

Initial Evaluation of a New Axial Flow Pump, Inserted by Minimally Invasive Thoracotomy, to Maintain Cardiac Output in a Porcine Model of Cardiogenic and Hemorrhagic Shock (Frazier, Radovancevic)

15. Project II.F..... 43

Physiological Magnetic Resonance Imaging (Willerson, Litovsky, Naghavi)

16. Project III.A..... 53

Induction of Chemokine Expression in Endothelial Cells by C-Reactive Protein (Yeh)

17. Project III.B..... 55

Nitrotyrosine Formation, Metabolism and Function: Functions of Nitric Oxide and Nitrotyrosine in Shock, Sepsis, and Inflammation (Murad)

18. Project III.C..... 61

Genes Regulating Wound Healing and Susceptibility to Oxidative Injury (Geng)

Project I.A.

Administrative Section

Investigators: James T. Willerson, M.D.
S. Ward Casscells, M.D.

For DREAMS:STAT, we have utilized Administrative funds for providing assistance, coordination of the various research programs, statistical analysis assistance, and miscellaneous items required by various investigators in this project.

All salaries are in accordance with the policies and procedures of the University of Texas-Houston Health Science Center. Fringe benefits are calculated at a rate of 21.5%.

Dr. Ward Casscells is the Principal Investigator for DREAMS:STAT and some financial support for his level of effort is budgeted in this section. Dr. James Willerson is an Associate Principal Investigator and financial support for his level of effort is also included in the budget. Scott Harrison is the Administrator for the DREAMS-STAT program. He coordinates research schedules, administrative reports, purchasing activities, and serves to help each investigator solve administrative problems that arise. Funds are also budgeted for statistical assistance for data evaluation in each of the research sections and for office supplies, including paper, pencils, pens, as well as storage items, computer costs, and such for each of the investigators.

Again, DREAMS:Science, Triage, and Treatment (STAT) well exceeded expectations, as there were more fundamental discoveries and practical inventions, mostly in the areas of tissue injury, inflammation, infection, and imaging. Publications, patents, presentations, and awards were numerous and exceeded those of DREAMS:STAT 2001. One project from the 2001 work has been excluded for 2002 (Gene Transfer of Tissue Factor Pathway Inhibitor), as no funds were allocated for the continuation of this work. Drs. Willerson and Casscells concluded that the key goals of the aforementioned project were no longer parallel with the overall objectives set forth by DREAMS-STAT.

Several DREAMS technologies continue to undergo testing in clinical trials. The first is a thermography catheter for detection of vulnerable atherosclerotic plaques by the heat they emit, a DREAMS-STAT finding that has won several awards and has led to the start-up of at least four companies. The University of Texas and the Texas Heart Institute licensed the patents of Drs. Casscells, Willerson, and Naghavi to one of these, Volcano Therapeutics. Over 100 patients have already been studied in clinical trials in three countries and European approval has already been issued. The US trial is now underway and FDA approval is expected in early 2004.

The project on hypothermia has also led to new inventions with one patent recently issued and five more being filed. This technology now promises to enable surgeons, pulmonologists, anesthesiolgists, anesthetists, nurses and medics to monitor injured or infected patients or those with heart or lung disease. The catheter is inserted under local or general anesthesia from the internal jugular vein to the apex of the right ventricle where it monitors the bipolar EKG, temperature, pressure, pO2, pH, and pCO2. This is expected to enable automated real-time diagnosis and monitoring of sepsis, myocardial ischemia, heart failure, respiratory failure and renal failure. The technology has led to a device start-up, LifeSentry,Inc.

Of particular relevance to the critical role of the USAMRMC in bioterrorism, DREAMS PI Dr. Casscells founded DefenseOfHouston, the citizen group that on September 6, 2002 was awarded the Best Practice Award of the US Department of Health and Human Services. Dr Casscells was chosen to serve on several task forces including the Mayor's Advisory Committee to the Medical Strike Team, the Houston Task Force on Terrorism, The University of Texas Homeland Security Committee, the Governor's Council on Health and Bioterrorism, the Pharmacology and Vaccine task force of the Center for Strategic and International Studies in Washington, and the Bush-Cheney Healthcare Advisory Committee.

In 2004, we aim to initiate our newest research endeavor, T5: Texas Training and Technology Against Trauma and Terrorism. This comprehensive project will continue to develop the basic biology and technology needed to improve the care of battlefield injuries. All T5 investigators look forward to a prosperous and exciting year of research in 2004.

The DREAMS-STAT investigators are thoroughly grateful for the financial support provided by the United States Army for carrying out this research. We are sincerely honored to be working with United States Army and look to further advance the knowledge of battlefield medical care with the Army's needs in mind.

Project I.B.

Mechanisms of Cardiomyocyte Injury in Shock

Investigator: L. Maximilian Buja, M.D.

Introduction: Endotoxic shock leads to profound and diverse effects in mammalian cells. One clinically important consequence of endotoxic shock is the death of cardiac myocytes. Lipopolysaccharide (LPS, endotoxin) is a major component of bacterial cell walls and the major instigator of cellular responses that lead to endotoxic shock. We have previously reported the existence of an innate protective phenotype in the neonatal heart against endotoxin induced cell death. In the adult heart, cardiac resistance to endotoxic shock occurs after a "preconditioning" exposure to sub-lethal doses of endotoxin. We proposed that these two observations indicate that the protective mechanisms operative in the neonatal heart can be reactivated in the adult heart to protect against cell death. This protection may require changes in the expression of protective genes. These genes could represent potential targets for pharmacological interventions.

Our earlier results indicate that LPS treatment of neonatal myocytes led to the following observations:

- A direct increase in signaling through the NFκB pathway in the neonatal myocyte. Inhibiting this activation was sufficient to elicit cell death in response to LPS treatment.
- Although we also observed an increase in the activation of the Akt/PKB pathway in response to LPS, the use of specific inhibitors enabled us to report that activation of this pathway was not sufficient to elicit the NFκB response and cardio-protection.
- We also reported that protection against endotoxic cell death is attenuated by the anti-inflammatory cytokine, CydPGJ2. Production of this cytokine is mediated by both cyclo-oxygenase (COX) 1 and 2 pathways. However, the exogenous levels of this cytokine required is pharmacological and at least an order of magnitude greater than endogenous production.

- LPS leads to a transient loss of the mitochondrial membrane potential ($\Delta\Psi$).
- Myocytes exposed to LPS also demonstrate a rapid activation of p38 MAPK and ERK1/2.

These later two novel and exciting observations provided the basis for our most recent investigations of cardiac protection against LPS injury and form the basis for this report.

Recent Progress: Opening of the mitochondrial permeability pore (MPT) is proposed to lead to the release from the mitochondria of small molecules and the dissipation of the mitochondrial membrane potential, $\Delta\Psi$(1). Programmed cell death,or apoptosis, is proposed to be initiated by the loss of cytochrome c through the MPT. We have reported that this mechanism of cell death, as assessed by caspase 3-like protein activation, is operative in LPS-treated myocytes when NFκB activation is blocked by CydPGJ2. Others have proposed that a transient decrease in $\Delta\Psi$ may be cytoprotective by:

- Reducing mitochondrial Ca^{2+}.
- Reducing the mitochondrial production of reactive oxygen species.

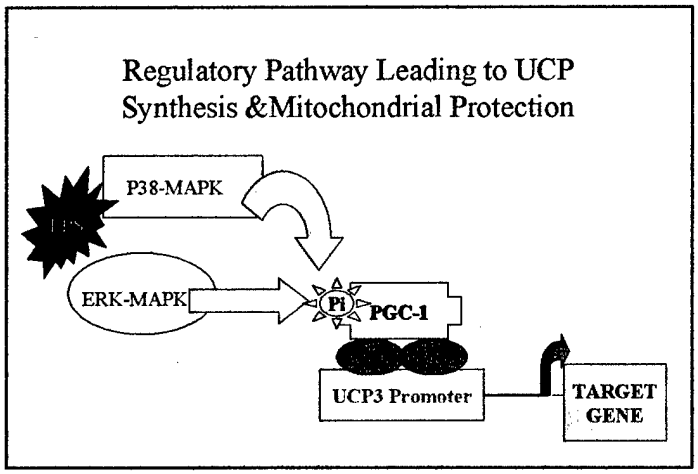

Figure 1: Pathway of UCP synthesis and mitochondrial protection.

Uncoupling proteins (UCP's) are named for their ability to uncouple ATP production from oxidative phosphorylation. The mechanism by which these proteins act is not fully understood but involves a facilitation of a proton leak across the inner mitochondrial membrane.

After observing the transient decrease in $\Delta\Psi$ and the activation of ERK and p38 we proposed a mechanism whereby these proteins would regulate the expression of UCP 3 in the heart (Figure 1). In the period covered by this report we have extended our investigations on the issues raised by these observations.

1. LPS treatment of neonatal myocytes leads to a rapid mitochondrial loss of $\Delta\Psi$. This loss is reversible and $\Delta\Psi$ is recovered within 20 hours.

After incubation with sub-lethal levels of LPS for an appropriate time the cells were labeled with the potential sensitive dye, MitoTracker Red. Energized mitochondria can then be visualized by confocal electron microscopy (Figure 2). Perinuclear mitochondria become energized before peripheral mitochondria (see 4 hours).

2. The levels of UCP3 increase within the myocyte rapidly after LPS treatment (Figure 2).

This increase occurs on the same time scale as the decrease in $\Delta\Psi$ (Figure 2) and temporally is subsequent to the NFκB activation noted in previous reports. UCP-3 expression levels are low when $\Delta\Psi$ is high. After treatment with LPS expression of UCP-3 increases then decreases as the number of energized mitochondria increase.The distribution of the expressed UCP3 is perinuclear. Modeling and co-localization are now being used to determine whether this expression is coincident with perinuclear mitochondria.

3. Cellular expression of UCP 2 also increases but shows different kinetics than UCP3 (Figure 3).

Differences in the expression of these proteins was also observed in skeletal muscle of mice treated with LPS (2). While the temporal changes in UCP-3 expression are inversely related to the number of energized mitochondria the expression of UCP-2 increases in manner similar to the myocyte production of TNFα (Figure 4).

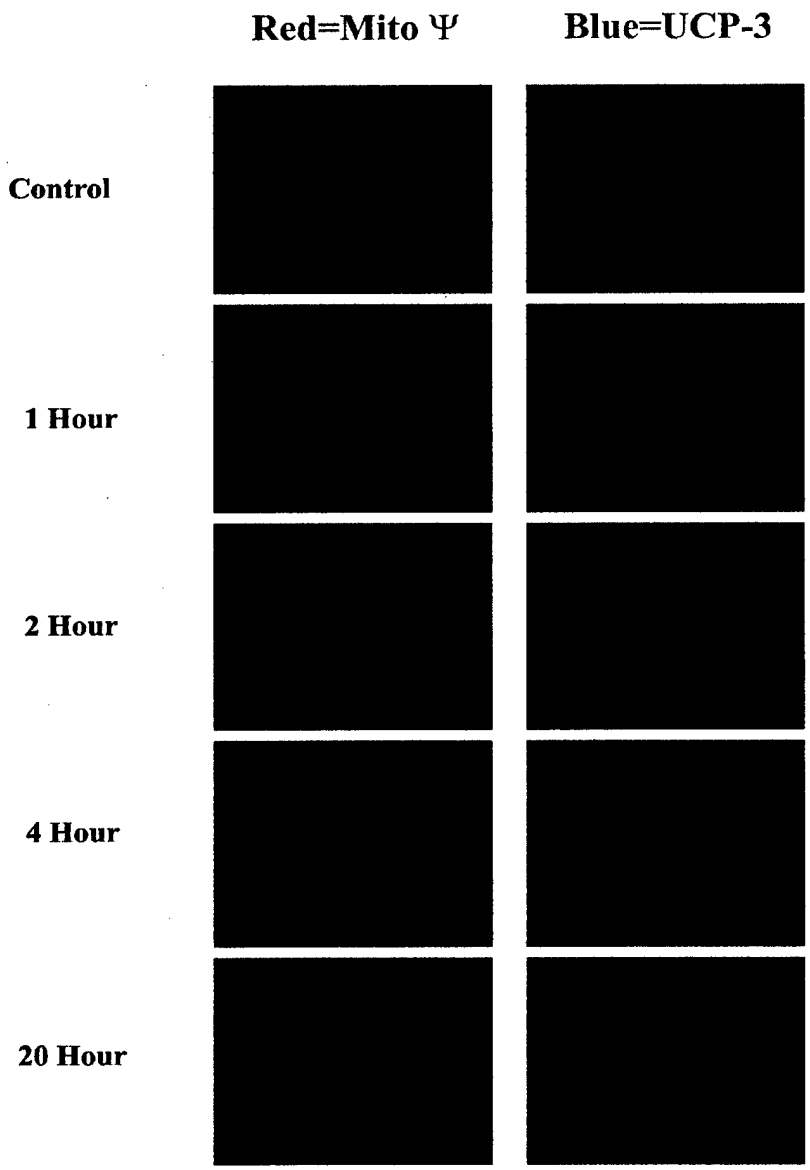

Figure 2: Loss of Mitochondrial Membrane Potential and an Increase in UCP-3 Follow Early Exposure to LPS. $\Delta\Psi$ was monitored using the potential sensitive dye MitoTracker Red. UCP-3 protein was identified by immuno-staining using a fluorescent Cy-5 secondary antibody.

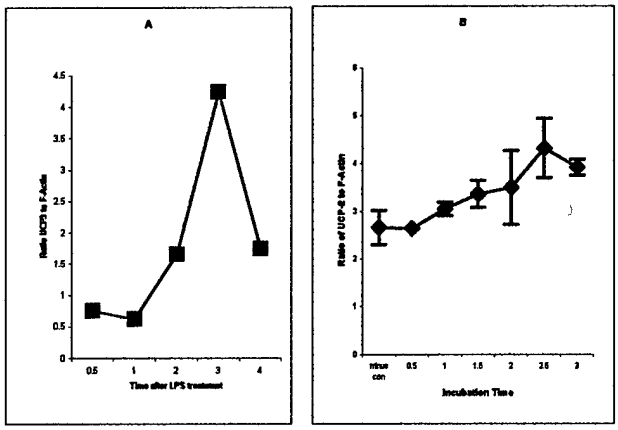

Figure 3: Protein levels of UCP-3 (A) and UCP-2 (B) after LPS treatment.

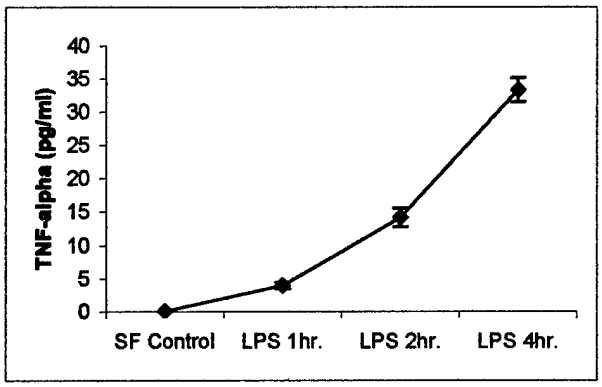

Figure 4: TNFα levels after LPS treatment.

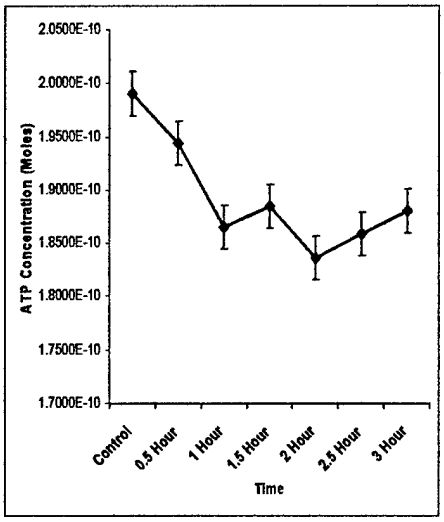

Figure 5: ATP synthesis decreases following exposure to LPS.

4. ATP levels within cells treated with LPS show a rapid and significant decline (Figure 5).

5. No changes were observed in the protein expression levels of PGC-1 (data not shown).

Conclusions: Our data suggest that the observed transient loss of mitochondrial membrane potential is closely associated with an increase in the expression of UCP-3. Expression of PGC-1 does not change within this time frame making our model proposed in Figure 1 incorrect. Loss of $\Delta\Psi$ is also associated with a decrease in cellular ATP levels as the cell consumes ATP as it attempts to restore the proton gradient. UCP-2 expression does not appear temporally associated with the loss of mitochondrial $\Delta\Psi$ and may be associated with an increase in TNFα production as previously reported in liver, skeletal muscle and white adipose tissue (3). How the cell regenerates energized mitochondria is of great interest. Since an energy source in required to regenerate the proton gradient this would only be possible if the ATP level is not allowed to drop below a threshold level.
Thus, LPS treatment of neonatal myocytes leads to an upregulation of NFκB, UCP-3 and, on a longer time scale, UCP-2 and TNFα. Blocking NFκB upregulation abrogates the protection of neonatal cells to LPS induced cell death. We propose that upregulation of NFκB is instrumental in increasing the expression of UCP-3, by a mechanism not requiring increased PGC-1 expression. Increased UCP-3 expression leads to uncoupling of the mitochondria and protection of the cell from the production of ROS. Alternatively, loss of mitochondrial $\Delta\Psi$ may protect the mitochondria from Ca^{2+} overloading and ensuing cell death.
These studies have identified novel potential targets for pharmacological intervention to prevent LPS induced cell death in the heart. Interventions that increase cardiac UCP-3 expression could prove protective.

Ongoing Studies: We are currently trying to dissect the mitochondrial response to LPS. If our hypotheses are correct then blocking NFκB should prevent the increase in UCP-3 expression and the loss of $\Delta\Psi$. Mitochondrial ROS production and Ca^{2+} changes will also be monitored by

confocal microscopy after treatment of these cells with LPS.

References:

1. Crompton, M. (1999) *Biochem J* **341 (Pt 2)**, 233-249
2. Yu, X. X., Barger, J. L., Boyer, B. B., Brand, M. D., Pan, G., and Adams, S. H. (2000) *Am J Physiol Endocrinol Metab* **279**, E433-446
3. Faggioni, R., Shigenaga, J., Moser, A., Feingold, K. R., and Grunfeld, C. (1998) *Biochem Biophys Res Commun* **244**, 75-78

Project I.C.1.

Molecular Regulation of Apoptosis in Wound Healing

Investigator: Yong-Jian Geng, M.D., Ph.D.

Specific Aim: This project was aimed at clarifying the molecular mechanisms underlying apoptosis of inflammatory cells and vascular cells induced by oxidative stress during wound healing. In this period, we conducted and accomplished the following experiments:

Major Findings: Stress or heat shock induced attenuation of nitric oxide synthesis is mediated by the actin-associated protein gelsolin in vascular smooth muscle cells stimulated with proinflmmatory cytokines.

Expression of inducible nitric oxide synthase (iNOS) responsible for the high output pathway of NO production that can cause apoptosis occurs in many inflammatory tissues and cell types, such as atherosclerotic arteries. Because these tissues and cells also express high levels of stress proteins such as heat shock proteins, we tested whether heat shock proteins affects expression of iNOS in vascular smooth muscle cells stimulated by proinflammatory cytokines, e.g. interferon gamma (IFN-γ) and tumor necrosis factor alpha (TNF-α). On the other hand our previous work has demonstrated that gelsolin, an actin-binding protein, contributes to several events triggered by activated caspases during apoptosis of vascular smooth muscle cells. Local induction of iNOS has been implicated in association with vascular damage, apoptosis, and inflammation.

We therefore investigated whether gelsolin-deficiency alters iNOS expression in heat shocked smooth muscle cells. Gelsolin-null and wild type mouse aortic SMC grown at subconfluence were assigned to either heat therapy or a control group. The cells of stress and control groups were incubated with the DMEM medium with 10% fetal bovine serum at 37°C. The stress group was exposed to the medium pre-warmed and maintained at 42° C for 15 minutes. The control group was treated in the same way except for the temperature setting at 37°C. Two hours after thermal stimulation, SMC were treated with TNF-α (10ng/ml) in the

presence or absence of IFN-γ (10ng/ml). After cytokine treatment, nitrite, an end product of NO in the culture media was measured by use of Griess' reagent and total proteins were extracted from SMC for iNOS, HSP and □-actin immunoblotting.

Compared to the control cells, cells stressed by thermal stimulation showed a marked reduction in nitrite production. Immunoblotting with anti-iNOS demonstrated a reduced intensity of iNOS bands in the stress group. Viability assays with fluorescent dye staining revealed no significant decline in viable cell numbers suggesting that the reduction in iNOS expression was not due to cell death. We further observed that the heat stress markedly induced expression of HSP70, but showed no effect on SM-α-actin expression. Interestingly, we observed that the thermal stress-induced suppression of iNOS was significantly attenuated in gelsolin-null cells. We detected that cytokine stimulation dose-dependently increased nitrite production (Fig. 1) and iNOS expression (Fig. 2) in vascular smooth muscle cells.

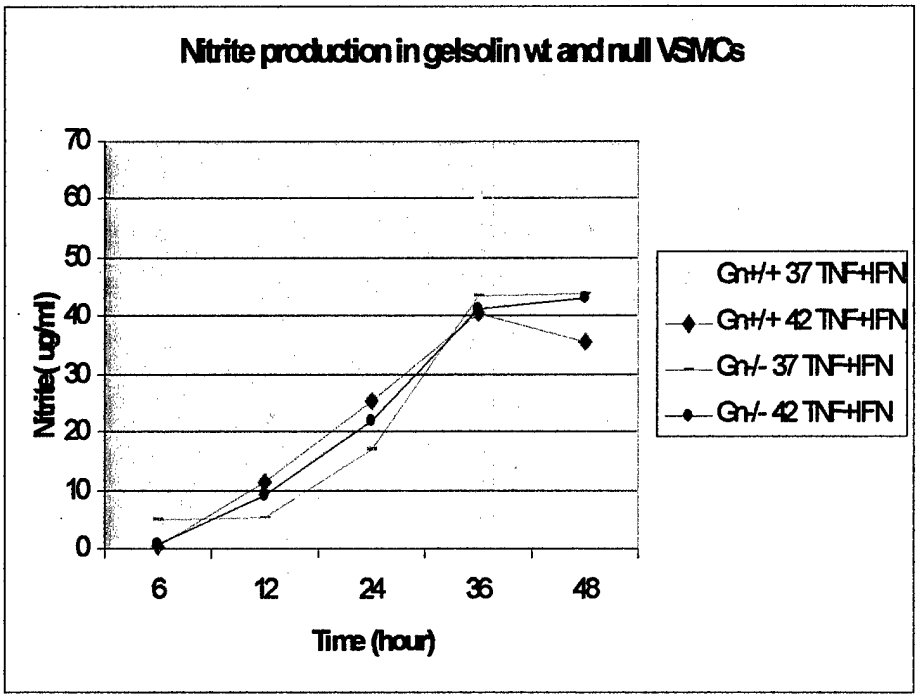

Figure 1. Nitrite production in gelsolin-positive (Gn+/+) and negative (Gn-/-) vascular smooth muscle cells (VSMCs) preheated at 42oC and then stimulated with the proinflammatory cytokines (TNF-α and IFN-γ).

Preheating the cells for 15 min significantly reduced nitrite synthesis and iNOS protein expression in wild type cells. However, interestingly, we found that the inhibitory effect of heat shock on nitrite synthesis gelsolin-null smooth muscle cells was abolished almost completely. In the gelsolin-nul cells preheated at 42°C, expression of iNOS proteins appeared to be at the same levels as those cultured at 37°C. In conclusion, heat shock-induced reduction of nitrite production and iNOS expression requires gelsolin expression. This finding reveals a novel biological role for geloslin in regulation of intracellular signaling.

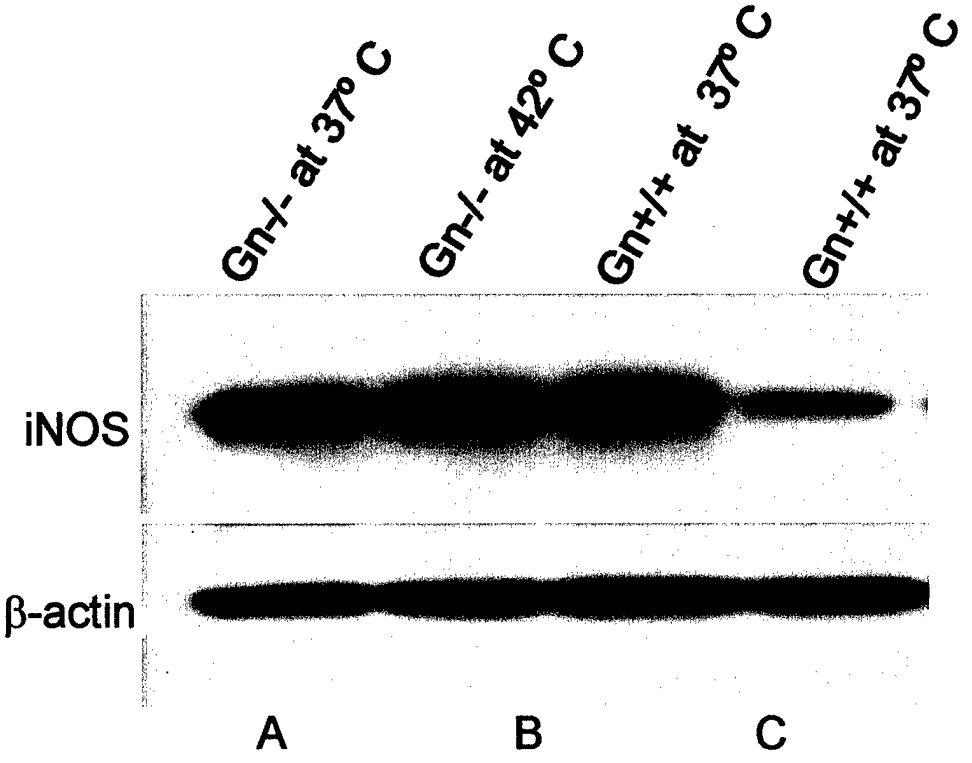

Figure 2. Western blot for inducible nitric oxide synthase (iNOS) in gelsolin-negative (Gn-/-) and positive (Gn+/+) vascular smooth muscle cells preheated at 42°C and then stimulated with the proinflammatory cytokines, IFN-γ and TNF-α(10 ng/ml, each).

Project I.C.2.

Infrared Spectroscopic Diagnosis of Vulnerable Atherosclerotic Plaque

Investigator: S. Ward Casscells, M.D.

Introduction: Near-infrared chemometric assays appear to be ideally suited for measuring both the *in vivo* size, composition, and relationships of the vulnerable structural components (fibrous crown, lipid reservoir, macrophage content) as well as clinically relevant vulnerable blood markers such as c-reactive protein (CRP).

Typically, vulnerable plaques do not cause high-grade stenosis and are therefore invisible to all current clinical diagnostic techniques. The fibrous crown is thin due because of its relative position it is close to the surface, and therefore close to an intravascular near-IR catheter. The lipid reservoir, while deeper, is larger and has specific signals where there is minimal interference and the penetration of near infrared light is able to reach this deeper portion. The most important aftermath of plaque rupture is thrombosis.

Detection of susceptible plaques is clinically relevant in that the detection of these specific plaques enables the clinician to better diagnose and manage the patient presenting with chronic coronary artery disease. The chemical information obtained will eventually be used in comparing the relative benefits of aggressive therapies (e.g., stents, drugs like matrix metalloproteinase inhibitors, or radiation) aimed at plaque stabilization and revascularization in the control of chronic coronary artery disease.

The purpose of the current study was to test the hypothesis that dynamic near-infrared chemical analysis utilizing a fiber optic catheter is capable of detecting vulnerable structural components within arterial walls in vitro (human).

Experimental Methods:

In Vitro Human Studies:

Human aortic plaques were obtained systematically from 6 different explanted aortas at the time of post-mortem analysis. Aortic wall circumferential strips, 50 mm in length and 10 mm in width were used. Each strip was fixed in 10% buffered formalin and cut into segments 3 mm in width for near-IR spectrometric analysis. Following NIR scanning, tissue samples were processed into paraffin blocks and analyzed by histology for presence or absence of lipid reservoir, thin fibrous crown (thickness< 65 μm by ocular micrometry), and macrophage infiltration. Specimens were stained by the hematoxylin/eosin and elastic trichrome combination technique, and evaluated by optical microscopy according to the American Heart Association (AHA) plaque classification. Samples too damaged for histological analysis or NIR analyses were discarded prior to any studies.

Reference Assay for Lipid and Fibrous Content:

For plaque chemical reference analysis and spectral correlations, excised plaques were quickly rinsed in Kreb's physiological salt solution to remove adherent LDL and oxLDL before being frozen in liquid nitrogen. An aliquot of plasma or tissue extract was diluted with a 50 mM phosphate buffer containing the following preservatives (buffer A): 2.7 mM EDTA, 2 mM benzamidine, 10 microM probucol, 1 microM PPACK, 0.01% aprotonin, 0.008% chloramphenicol, and 0.008% gentamycin, 1 mM PMSF, 1 mM leupeptin, and 40 mM elastinal. For the tissue plaque extraction, plaque segments were cut into small pieces (~1 mm) in a cooled, nitrogen-purged glove box while under the de-gassed extraction buffer using an immersible tissue chopper. Minced tissue was then extracted overnight at 4oC under nitrogen using an orbital shaker (10 rpm) in 0.14 M NaCl/0.01 M phosphate buffer, pH 7.2, containing the preservatives as in buffer A. The extract was collected by low-speed centrifugation at 4 °C, washed once with extraction buffer, and the supernatants combined. The supernatant was transferred into 12-ml tubes, overlayered with 0.5 ml of water, and centrifuged at 100,000g for 30 min at 5 °C. LDL (density, 1.019-1.063 g/ml) was isolated from plasma and plaque extracts by density-gradient ultracentrifugation over a potassium bromide gradient at 200,000g (4 hours at 22 °C). The LDL fraction (density of 1.019-1.063, determined by light illumination)

was obtained and dialyzed overnight at 4oC against 0.14 M NaCl/0.01 M phosphate buffer (pH 7.4) containing 0.27 mM EDTA and 1 mM PMSF. After dialysis, the LDL fraction was sterile filtered and stored under nitrogen at 4oC. Protein content was determined according to Bradford's method. For comparison, commercial LDL (Sigma, St Louis) and oxLDL (LDL oxidized in the presence of 10 mM copper sulfate at 37 °C for 24 hrs) were used as reference standards. A calibration curve was constructed for the near-IR spectra of freshly prepared ox-LDL to allow quantitative determination of ox-LDL.

Reference assays for plasma and tissue extracts consisted of SDS-PAGE and measurement of thiobarbituric acid reactive substances (TBARS). Before electrophoresis, the samples were prepared in a buffer containing 0.063 M Tris-HCl, 2% SDS, 10% glycerol, 10 ÊM BHT, and 0.001% bromphenol blue (pH 6.8) and heated for 3 min in a boiling water bath. SDS-PAGE was performed using 4-12% gradient gels (100 V, 30 mA for 75 min; Protean 2 mini gel electrophoresis system, Biorad, CA) in a running buffer containing 0.025 M Tris, 0.19 M glycine buffer, pH 8.3, containing 0.1% SDS. Coomasie brilliant blue or silver stains were used to visualize protein bands. Each stained gel containing extracted plaque lipoproteins was digitized using a Si CCD imager, and absorbance values were calculated for the bands in each lane. The bands on the gels were identified and quantified using molecular weight markers (broad range, Biorad, CA), commercial LDL, and ox-LDL standards on each gel.

In Vitro NIR Spectroscopy of Human Plaques:

In vitro human aortic plaques were scanned under a near-IR fiber optic probe and conducted in a nitrogen-purged glove box at 4 °C. The optical window in the glove box was maintained at -20 °C for the frozen plaques, which were scanned immediately before chopping and biochemical extraction). Collagen and elastin in the fibrous cap were determined via histological examination by serial paraffin-embedded sections (5 mm) stained with Sirius red or orcein for collagen and elastin visualization.

NIR Spectral Analysis:

After multiplicative scatter correction and smoothing the 1-D spectra from the slices, principal axis transformation

was employed to create a loadings (or transformation) matrix. The reference assay results were used to isolate the vectors in this matrix (principal components) that correlated to each reference assay. Inverse principal axis transformation using only the relevant vectors of the loadings matrix created spectra corresponding to each reference.

Results: Macrophage content was determined histologically and the NIR spectra were calculated from inverse principal axis transformation using only the principal components that correlated to the selected reference assays. The water band at 5155 cm^{-1} in the fibrous crown was anti-correlated to the saturated lipid band at 4330 cm^{-1} in the reservoir. The saturated lipid band at 4330 cm^{-1} in the fibrous crown was correlated to the saturated lipid band at 4330 cm^{-1} in the reservoir. The amide band at 4810 cm^{-1} in the fibrous crown was correlated to the amide band at 4810 cm^{-1} in the lipid reservoir. The -CH2- lipid band at 5880 cm^{-1} was anti-correlated to the amide band at 4810 cm^{-1}. The -CH2- lipid band at 5880 cm^{-1} was anti-correlated to the band at 7410 cm^{-1}, while the saturated lipid band at 4385 cm^{-1} was positively correlated. These features tend to repeat in spectra of most of the nominally susceptible plaques scanned, and led to the good performance of the HELP algorithm in prediction of plaque characteristics below.

Near-IR predictions by HELP of fragile fibrous crown, lipid reservoir, and macrophage infiltration in human aorta segments in vitro were compared with results by histological examination. Each binary variable (i.e., lipid reservoir present=1, absent=0) was correlated to the NIR spectra. The results are shown below.

Sample	Positive	Negative
Lipid	92% correct	100% correct
Fibrous	89% correct	100% correct
Macrophage	85% correct	100% correct

Project I.C.4

Nitric Oxide in Organ Failure

Investigator: Bruce C. Kone, M.D., FACP, FCP

Summary: The broad goals of this project are to determine the molecular basis underlying the effects of nitric oxide (NO), its derived reactive nitrogen intermediates, and other pro-inflammatory mediators to injure tissues during multiple organ failure and to design therapeutic interventions to protect against this injury. Acute ischemia and reperfusion (I/R) is a common consequence of post-traumatic shock and resuscitation characterized by local and systemic derangements, including dramatic induction of NO along with other pro-inflammatory genes that may result in multiple organ failure.

Work during the previous funding period in our laboratory using a rat model in which gut injury and multiple organ failure are induced by 45 minutes of superior mesenteric artery occlusion followed by progressive periods of reperfusion identified differential phosphorylation of IkappaBalpha as a key signaling component leading to gut injury following mesenteric I/R. In addition, we demonstrated a remarkable effect of alpha-melanocyte stimulating hormone alpha-MSH), an endogenous anti-inflammatory peptide known to abrogate lung and liver injury in multiple organ failure, to protect the gut from I/R injury. Similarly, we determined that topical hypothermia applied to the gut during ischemia was also protective against I/R injury.

Results: To determine whether alpha-MSH might be effective during the reperfusion period, we tested the therapeutic efficacy of alpha-MSH on gut I/R injury when given at different time points of reperfusion. Rats underwent sham surgery or were treated with saline or with alpha-MSH given 1 h, 2 h, or 4 h after superior mesenteric artery clamping. Vehicle-treated I/R rats exhibited severe mucosal injury, and increased NF-kappaB DNA binding activity, myeloperoxidase activity, and IL-6 and heme oxygenase-1 expression. In contrast, rats given alpha-MSH at 1 h or 2 h of reperfusion, but not 4 h, exhibited much less mucosal injury and MPO activity, less NF-kappaB DNA binding

activity and IL-6 protein, and even higher levels of heme oxygenase-1. These effects were most prominent in rats treated with alpha-MSH at 1 h of reperfusion. Thus, alpha-MSH, an endogenous peptide with a favorable side-effect profile, is effective in treating experimental gut I/R injury when given early *after* the initial ischemia, and may represent a candidate therapy for gut I/R in humans in whom recognition and treatment are often delayed. A manuscript reporting these findings is in press in Shock.

Given the distinctive actions of alpha-MSH, a known inhibitor of IkappaBalpha tyrosine phosphorylation, and BAY 11-7085, an inhibitor of IkappaBalpha Ser 32,36 phosphorylation, on modulating the course of gut I/R injury, we hypothesized that combined blockade of Ser and Tyr phosphorylation of IappaBalpha by co-administration of BAY 11-7085 and alpha-MSH would provide continuous protection at early (30 min) and late (6h) time points of reperfusion. Using the gut I/R model described above, we found that combined use of alpha-MSH with BAY 11-7085 abrogated gut myeloperoxidase induction and tissue injury at both time points, whereas we had previously found that either compound given alone produced histologic protection and limited myeloperoxidase activity in either early or late reperfusion, but not both. Our new data thus suggest that suppression of both Ser 32 and 36 phosphorylation (by BAY 11-7085) and late Tyr phosphorylation (by alpha-MSH) of IkappaBalpha abrogates gut I/R injury during different phases of reperfusion injury. A manuscript reporting these findings is in press in Shock.

We also extended our results of therapeutically applied intraischemic hypothermia, which we have found protects the gut during mesenteric I/R. We examined the role of heme oxygenase-1 in a more severe model of gut I/R injury produced by 75 min of SMA occlusion and 6 h of reperfusion, which results in more persistent gut dysfunction as indexed by intestinal transit at 24 h of reperfusion. Heme oxygenase-1 protein expression in the ileum of the gut I/R rats was more than twice that of sham animals. Rats treated with intraischemic topical hypothermia exhibited even greater levels, by ~50%, of heme oxygenase-1 protein in the ileum compared to the normothermic I/R controls, and had preserved histology and transit. To implicate functionally heme oxygenase-1 in the protective response, rats were treated with the heme oxygenase-1 inhibitor Sn-protoporphyrin IX (25 □mol/kg IP) 1h prior to SMA occlusion. Sn-protoporphyrin IX exacerbated I/R-induced

histological injury and impaired transit but abrogated the protective effects of intraischemic topical hypothermia on these parameters. We concluded that hypothermia protects against gut I/R-induced impaired intestinal transit by inducing heme oxygenase-1. A manuscript reporting these results is in press in Journal of Surgical Research.

During the previous funding cycle, we identified a novel mechanism for termination of NO production in cytokine stimulated mesangial cells in which signal transducers and activators of transcription 3 (STAT3), via direct interactions with NF-kappaB, serves as a dominant-negative inhibitor of NF-kappaB activity to suppress cytokine induction of iNOS transcription. STAT3 is a modular protein with several structurally and functionally defined domains. To define the specific domains of STAT3 that interact with NF-kappaB p65, we synthesized ^{35}S-labeled proteins corresponding to each STAT3 domain and tested their ability to bind specifically a GST-NF-kappaB p65 fusion protein in the GST pull-down assay. The coiled-coil (CCD) and DNA-binding (DBD) domains were specifically retained by GST-NF-kappaB p65, whereas the N-terminal, linker, SH2, and transcriptional activation domains did not interact with NF-kappaB p65. Deletion of the region L^{358} through I^{368} of the STAT3 DBD greatly reduced binding, indicating that this region is necessary for GST- NF-kappaB p65 binding. Alanine substitution mutations at four highly conserved residues (L^{358}, N^{359}, K^{363}, and V^{366})in this region virtually abolished NF-kappaB p65 binding. In contrast to the trans-repression of iNOS promoter activity afforded by wild type STAT3, overexpression of full-length STAT3 harboring these mutations failed to trans-repress an iNOS promoter-reporter construct in mesangial cells. Taken together, our data reveal a novel role for the DBD and CCD domain in the physical and functional coupling to NF-kappaB p65 that appears to be important for regulating iNOS and likely other NF-kappaB p65-responsive genes in mesangial cells. A manuscript reporting these results is under review, and an abstract has been selected for presentation at the November 2003 Annual Meeting of the American Society of Nephrology.

Key Research Accomplishments:

- Demonstration that administration of alpha-MSH even one hour after the initial ischemia abrogates gut I/R injury and, like topical hypothermia, results in a sustained increase in heme oxygenase-1 expression.

- Demonstration that the combination of Alpha-MSH and BAY 11-7085, attenuated gut I/R injury at both early and late time points of reperfusion.
- Demonstration that intraischemic hypothermia topically applied to the gut abrogates I/R injury in part by inducing heme oxygenase-1 activity.
- Demonstration of the binding domains of STAT3 with NF-KappaB responsible for inhibition of iNOS transcriptional activation.

Reportable Outcomes:

Articles:

Hassoun, H.T., Kozar, R.A., Kone, B.C., Safi, H.J., and Moore, F.A.: Intraischemic hypothermia differentially modulates oxidative stress proteins during mesenteric ischemia/reperfusion. Surgery 132:369-376, 2002.

Zhang, S., Yang, Y., Kone, B.C., Allen, J.C., and Kahn, A.M. Insulin-stimulated cyclic guanosine monophosphate inhibits vascular smooth muscle cell migration by inhibiting Ca^{2+}/calmodulin-dependent protein kinase II. Circulation 107:1539-1544, 2003.

Zou, L., Attuwaybi, B., and Kone, B.C. Effects of NF-□B inhibition on mesenteric ischemic-reperfusion injury. Am. J. Physiol. 284:G713-G721, 2003.

Kuncewicz, T., Sheta, A., Goldknopf, I., and Kone, B.C. Proteomic analysis of S-nitrosylated proteins in mesangial cells. Mol. Cell. Proteomics 2:156-163, 2003.

Attuwaybi, B.O., Hassoun, H.T., Zou, L., Kozar, R.A., Kone, B.C., Weisbrodt, N.W., and Moore, F.A. Hypothermia protects against gut ischemia/reperfusion induced impaired intestinal transit by inducing heme oxygenase-1. J Surg Res, in press.

Zou, L., Sato, N., Attuwaybi, B.O., and Kone, B.C. Delayed administration of □-MSH or combined therapy with BAY 11-7085 protects against gut ischemia-reperfusion injury. Shock, in press.

Abstracts:

Yu, Z-Y., and Kone, B.C. STAT3 DNA-binding and coiled-coil domains physically and functionally interact with NF-□B p65 to regulate iNOS transcription in mesangial cells. 36th

Annual Meeting of the American Society of Nephrology, San Diego, CA, 2003.

Conclusions: Multiple organ failure is a common, often catastrophic outcome of combat-induced trauma. An improved understanding of the molecular basis for the initiation and amplification of cell and organ injury will ultimately inform the rational design of therapeutic agents to prevent, delay, or reverse post-resuscitation multiple organ failure. In the aggregate, our studies provide new insights into the early molecular events underlying both intestinal ischemia-reperfusion injury and multiple organ failure, new insights into the regulation of iNOS and NF-kappaB, and novel therapeutic strategies to limit I/R injury and multiple organ failure.

Project I.C.6.

Is Hypothermia an Indicator of Imminent Death in Congestive Heart Failure and Helpful in Triage

Investigator: S. Ward Casscells, M.D.

Introduction: Work performed in hypothermia research extended to coronary sinus monitoring for indications of myocardial ischemia. The relationship of blood temperature changes in the coronary sinus resulting from upstream myocardial ischemia dovetails into the realm of hypothermia for triage assessment. Below are summaries of hypothermia studies in which we assesses core body temperature in congestive hear failure patients (CHF) and ischemia studies involving coronary sinus thermometry in patients undergoing percutaneous intervention (balloon angioplasty).

Core Body Temperature in CHF Patients: Most of the predictors of mortality described previously for patients with CHF have been difficult to monitor on an ambulatory and continuous basis, while others have been only modestly sensitive and specific. We had observed that low body temperature on admission may predict imminent death in hospitalized CHF patients and hypothesized that rapidly falling body temperature during hospital stay predicts in-hospital death well in advance in CHF patients.

Methods:

Using a nested case-control design, a cohort of 291 patients [age 73 years ±13, 53% women] were studied, chosen from 326 patients with a principle discharge diagnosis of CHF in the Memorial Hermann Hospital, Houston, Texas, January to December 1998, after excluding 35 patients with conditions known to confound temperature. Speed of body temperature change was calculated as the body temperature difference (°F) between two consecutive readings divided by time difference (hr).

Results:

During a mean hospital stay of 5 days ± 4, an average of 17 speed measurements per patient was recorded. Using repeated measures analysis of variance, between-subject variations among those 17 (6%) who died of cardiac causes and those who survived was significant ($p = 0.006$), while within-subject variations during the hospital stay were not ($p > 0.3$). A rate of temperature fall greater than 0.4 °F had the optimum sensitivity (52%, CI 95% 42-58) and specificity (58%, CI 95% 53-64) to predict death. Of the 17 patients who died, 8 had a speed of temperature fall greater than 0.4 °F for at least once during their hospitalization, and the time interval between the first time they had it and death had a mean of 112 hrs (CI95% 41-183 hrs).

Conclusions:

Falling body temperature predicted in-hospital death well in advance in CHF patients. The modest sensitivity and specificity of this predictive tool might be improved by more frequent and uniform measurements. The utility of ambulatory temperature monitoring merits further investigations.

Myocardial Ischemia Monitoring: In patients who might have otherwise undetectable episodes of myocardial ischemia, continuous monitoring might help detect such episodes and their frequency. We hypothesized that monitoring coronary sinus temperature (CST) can help diagnose myocardial ischemia, inflammation and evaluate cardiac energetics. We report preliminary results of a study on the effect of transient coronary occlusion on coronary sinus temperature.

Methods:

8 patients undergoing elective coronary angioplasty and stenting were enrolled in the study. CST was continuously recorded throughout the procedure in the proximal coronary sinus at the junction of coronary sinus and greater cardiac vein at a frequency of 100 times/ second with a sensitivity of 0.02°C using the temperature sensor of the Radi PressureWire (Radi Medical Inc., Reading, MA, USA). Statistical analysis was done using linear mixed effects models.

Results:

All patients were male, with mean age of 68 years (SD=10). Interventions (3 on native vessels and 5 on grafts) included deployment of drug eluting stents in all patients. The placement of the sensor wire in coronary sinus was done rapidly (< 1 minute in all cases) and uneventful. Following inflation of the balloon, CST significantly increased (mean adjusted increase of 0.20°C, $p<0.0001$). Upon restoration of coronary flow with the deployment of the stent, CST deceased below the baseline (mean adjusted decrease of 0.83°C, $p<0.0001$). One patient developed ST-elevation and 3 had chest discomfort during the procedure, and temperature increase preceded those in all cases. The procedure and the immediate follow-up were otherwise uneventful.

Conclusion:

A significant increase in coronary sinus temperature was associated with ischemia and preceded electrocardiographic changes and development of symptoms, and a fall in coronary sinus temperature was associated with the removal of ischemia. Use of these findings for monitoring of ischemia merits further investigation.

Project I.D.

Up-regulation of P450: A Natural, Broad-Based Defense Against Chemical and Biological Threats

Investigator: Henry W. Strobel, Ph.D.

The goal of this project has been to characterize the role of cytochrome P450 in response to chemical, biological and traumatic threats. In order to pursue this goal we have utilized RNA or protein samples or liver cells purchased from vendors or provided by collaborators.

Over the last year we have focused on the effects of traumatic injury or lipopolysaccharide (LPS) -induced inflammation on the regulation of Cytochromes P450 especially the CYP P450 4F subfamily. The cytochromes P450 undergo isoform specific alterations in expression following receipt of an inflammatory prompt (either injury or an infection modeled by LPS treatment) in a tissue-specific fashion. In other words, different P450 isoforms respond differentially to injury or LPS depending on the tissue under study. For instance, we have shown that in liver CYP 4F1 expression is not significantly altered after LPS treatment whereas CYP 4F4 is decreased by 55% and CYP 4F5 is increased by 60% whereas in kidney CYP 4F1 is unchanged, CYP 4F4 is not expressed in control or LPS treated samples and CYP 4F6 is unchanged (1). These changes in mRNA expression are consistent with total CYP 4F protein expression.

Treatment of rat hepatocyctes in culture for five days shows a dose-dependent inhibition of expression of each of the CYP 4Fs suggesting that the suppression seen in liver is mediated at the level of the liver cell rather than by cellular interactions. A 5ng dose of IL-1β brought about significant increases in CYP 4F1 and CYP 4F5 expression in hepatocyctes but a significant decrease in CYP 4F4 with no effect on CYP 4F6. Thus, the cytokine IL-1β treatment of hepatocyctes seems to mimic very closely the effects seen in liver RNA samples from rats treated with a single dose of LPS (1.0g/kg body weight).

RNA samples from rats receiving a controlled cortical impact to the temporal cortex showed a time-dependent decline in CYP 4F4 and CYP 4F5 expression reaching a nadir

at 24 hours post injury and recovering to a maximal expression at two weeks post-impact (2). Interestingly, the 24 hour time period at which CYP 4F levels are lowest is the time point at which cyclooxygenase II and Lipooxygenase 5 reach maximum expression whereas the reverse is true at two weeks.

These results are consistent with a 24-hour post injury inflammatory period where inflammation increases and a post 24-hour to two-week recovery period in which inflammation is combated and suppressed. Further, these results are consistent with the notion that the CYP 4F subfamily is a principal player in the recovery period since it is the only enzyme subfamily that effectively and efficiently removes the inflammatory prompts leukotriene B_4 and prostaglandins A_1 & E_1, the active products of lipoxygenase 5 and cyclooxygenase 2 activity respectively.

We plan to continue next year our study of the suppression of CYP 4F4 and CYP 4F5 in the inflammatory period to assess the coordinated regulation of the upregulation of cyclooxygenase 2 and lipoxygenase 5 with the down regulation of CYP 4F4 and CYP 4F5 during the inflammatory phase (the first 24 hours after injury).

Publications:

1. Kalsotra, A., Cui, X., Antonovic, L., Robida, A.M., Morgan, E.T. and **Strobel, H.W.**: Inflammatory prompts produce isoform-specific changes in the expression of leukotriene B_4 ω-hydroxylases in rat liver and kidney, *FEBS Letters*, In Press, 2003.

2. Cui, X., Kalsotra, A., Robida, A.M. Matzilevich, D., Moore, A.N. Boehme, C.L., Morgan, E.T., Dash, P.K. and Strobel, H.W.: Expression of Cytochromes 4F4 and 4F5 in Infection and Injury Models of Inflammation, *Biochemica et Biophysica Acta*, **1619**: 325-331, 2003.

Project I.E.

Detection and Quantitation of *Bacillus anthracis* in Macrophages

Investigator: Theresa M. Koehler, Ph.D.

Introduction: The spore-forming bacterium *Bacillus anthracis* is the causative agent of anthrax. Inhalation of large numbers of *B. anthracis* spores results in systemic anthrax disease, which is typically fatal. Inhaled spores are transported by alveolar macrophages to the mediastinal lymph nodes, where they germinate, produce an antiphagocytic capsule, multiply, and secrete the lethal anthrax toxin. Within a few days, symptoms progress from malaise and low fever, to dyspnea, cyanosis, high fever, and disorientation, to shock, coma, and death.

B. anthracis spore germination, the change from a dormant non-metabolic state to one of active metabolism and replication, is a critical early step in pathogenesis. It has been reported that alveolar macrophages appear to be the primary site for germination and putative germination genes have been identified (Guidi-Rontani, C. et al., 1999. *Mol. Microbiol.* 31:9-17; Guidi-Rontani, C. et al., 1999. *Mol Microbiol.* 33:407-14).

We propose to examine the physiology of *B. anthracis* growing in the context of a macrophage. In order to investigate the mechanisms by which germinated spores withstand the hostile environment of the macrophage and ultimately escape the macrophage, we need to be able to accurately measure growth of the bacterial cells in macrophages.

Results: Originally our intent was to assess *B. anthracis* germination and growth rates in macrophage cell lines. However, we have recently established collaboration with C. Rick Lyons of the University of New Mexico to assess *B. anthracis* pathogenesis in a mouse model for inhalation anthrax. We have decided to employ this animal model to examine *B. anthracis* development during infection. Toward this end, we have:

1) Determined that *B. anthracis* germinates in lungs of mice within 3 hrs following infection by the intra-tracheal route.
2) Begun experiments to assess *B. anthracis* gene virulence gene expression in the lung.

Germination & Dissemination of *B. anthracis* in Mouse Model

We inoculated five mice with 1 x 10^4 spores via the intra-trachael route. Lung tissue was harvested at the times shown in the figure. The data for time 0 indicate that 100% of the spores entered the lungs. Important conclusions from these experiments are:

- At 3-h post infection, 100% of the spores have germinated, as indicated by the isolation of heat-sensitive CFU.
- For the parent strain (UT500), vegetative bacteria could be detected in the spleen at 24 h. No spores were present in the spleen at any time during infection.
- A mutant strain (UT538), that is missing the biosynthetic genes for capsule synthesis, germinated as well as the parent strain, but did not disseminate to the spleen.

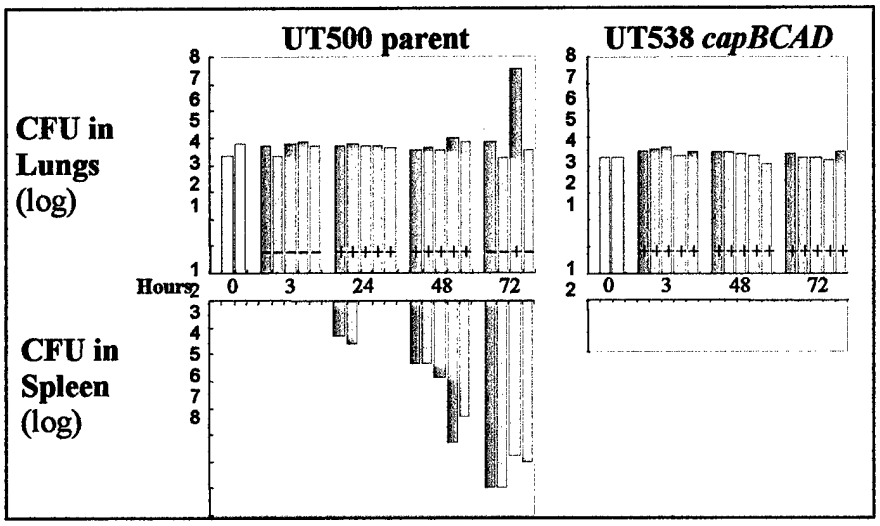

Figure 1. CFU detected in lung and spleen. In samples containing heat-resistant spores, these represented less than 5% of the CFU detected.
(+)heat-resistant spores present.
(-)heat-resistant spores not present.

B. anthracis Gene Expression in Mouse Tissue

Using non-quantitative PCR, we can detect expression of the capsule genes (*cap* mRNA) in lung and spleen tissue from mice infected with the virulent parent strain. We cannot detect this transcript in tissues from mice infected with the capsule null-mutant.

In our previous investigations, we developed real-time fluorescent quantitative PCR methods for quantifying specific *B. anthracis* DNA sequences in cell culture. In the last period, we have worked with the Quantitative Genomics Core Laboratory of the University of Texas - Houston Medical School to develop methods for measuring specific gene transcripts in tissue samples, such as lungs of infected mice. Since our tissue samples contain large amounts of mammalian RNA, we are concerned about the ability to detect low levels of bacterial RNAs in this background. We are currently examining the effect of mammalian RNA on detection of *cap* mRNA. As shown in the figure below, we have determined that our limit of detection for our Q-RT PCR assay is 10 pg/ul.

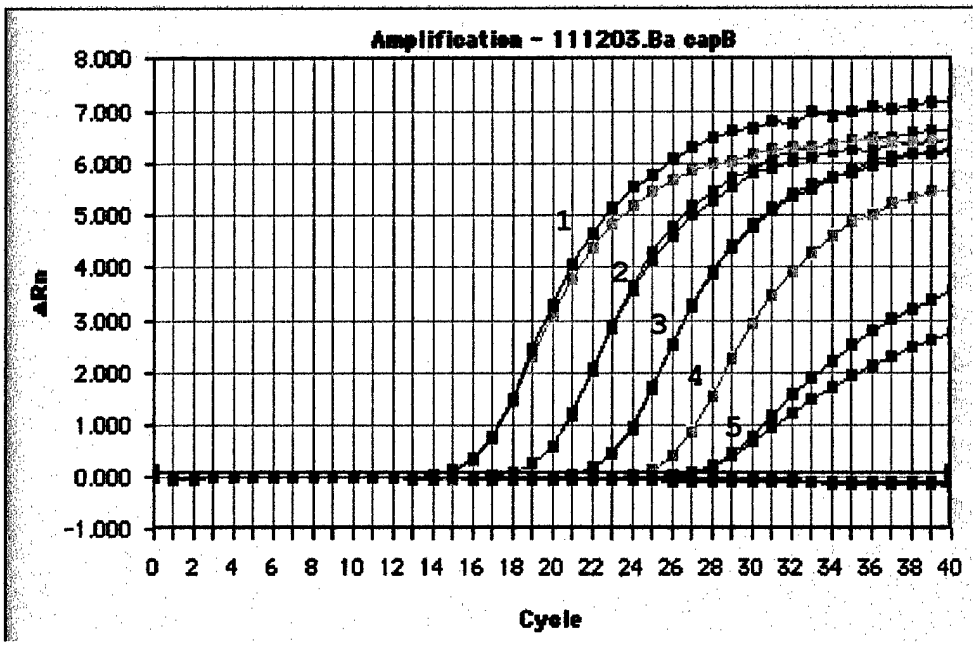

Figure 2. Amplification of B. anthracis mRNA using a quantitative RT-PRC assay. Serial dilutions are as follows: (1) 100 ng/µl, (2) 10 ng/µl, (3) 1 ng/µl, (4) 100 pg/µl, and (5) 10 pg/µl.

Key Research Accomplishments:

- Using a mouse model for inhalation anthrax, we have determined that *B. anthracis* spores germinate in the lungs within 3 hrs of initial infection.
- In the mouse model, capsule genes are required for dissemination of *B. anthracis* to the spleen.
- The limit of detection for bacterial transcripts (cap mRNA) is 10 pg/ul using our quantitative RT-PCR method.

Project II.A.
Pathology Core

Investigators: James T. Willerson, M.D.
L. Maximilian Buja, M.D.
Silvio H. Litovsky, M.D.

In the DREAMS program, we have continued to provide expert pathology assessment of various human and animal tissues that are obtained as part of the DREAMS research studies. Methods of analysis for these tissues include routine gross morphology, histology, lipid analysis, electron microscopy, immunohistochemistry, and quantitative morphometry. These techniques have been extremely useful in allowing investigators throughout the DREAMS program to evaluate tissues from experimental animal models to make quantitative determinations that allow them to test their hypotheses, develop their methods more exactly, and promote the development and refinement of new hypotheses.

The pathology core continues to interact extensively with the DREAMS investigators in order to get the maximum information from experimental protocols and thus, provide the best possible understanding of the pathology findings. These analyses are available for studies of tissues (i.e., experimental animal & human) that are obtained by investigators throughout the DREAMS project. In this particular part of the DREAMS program, we have again provided financial assistance for the efforts of Dr. Silvio Litovsky, who provide most of the analyses mentioned above, as well as support for the anatomic and laboratory pathology studies.

Project II.D.
Thermal Detection and Treatment of Inflammation and Necrosis

Investigator: S. Ward Casscells, M.D.

Introduction: In 2002-2003, we focused on the development of a thermobasket catheter for measuring the temperature of an arterial wall. The technique was adapted for in vivo studies in canine models and employed direct contact of thermal-sensing elements with the tissue of an arterial wall. The catheter was composed of nitinol with small, flexible thermocouples attached to the basket wires. The size was comparable to that of a 3F with an expandable, externally-controllable basket consisting of four flexible wires (each with a thermocouple). The catheter device was attached to a personal computer with a modified computer board and customized software for real-time, high-speed data acquisition, tracking, and thermal imaging. We also equipped the basket system with a central wire that had attached an additional thermocouple for measuring the blood temperature (as a calibration measure).

The goal of the work was to measure tissue temperature heterogeneities in the arteries of atherosclerotic canines. In regions devoid of atherosclerosis, we expected tissue temperatures to be homogeneous and "cool," whereas atherosclerotic lesions were expected to exhibit heterogeneous temperature variability and be "hot."

Experimental Design:

Bench Calibration Studies: Prior to in vivo studies, we thoroughly tested the catheter system to ensure operability and performance. Calibration of the catheter was performed in a circulating micro-bath showed concordance (±0.02°C) of all four thermal sensors. The four basket wires showed temperature measurements very close to the reference bath temperature (37°C) and multiple measurements by each wire showed high consistency with minimal coefficient of variation (0.0004, 0.000331, 0.000405, & 0.000453).

Phantom Simulation Studies: We also tested the catheter in a phantom system to proof the concept of detecting "hot" regions commensurate with inflamed atherosclerotic lesions. We were able successfully detect increased temperatures in our phantom and demonstrated thermal and spatial resolution. The washing (cooling) effect was proportionate to blood flow and was easily accounted for using the electronic feedback control. We postulated that tissue temperatures should be calibrated relative to the rate of blood flow.

Effect of Blood Flow and Luminal Narrowing: We observed that in medium-bore tubes simulating the non-stenotic coronary vessels that the average temperature measured by the peripheral wires in contact with the wall differed by 0.45-0.55°C from the central wire measuring the temperature of the flowing fluid. However, in small-bore tubes with low flow simulating coronary arteries with 95% stenosis, this difference was only 0.006 -0.015°C. This illustrates the potential of the catheter system to detect hot lesions in stenotic arteries.

Canine Model of Atherosclerosis: We tested the catheter system in an animal model of cholesterol-sensitive atherosclerotic dogs (developed by Dr. James T. Willerson through years of in-breeding). These canines are genetically susceptible to developing atherosclerosis after prolonged cholesterol feeding and generate significant lesions in certain locations, specifically the femoral arteries. Interestingly, they do not develop lesions in their carotid arteries. We tested the thermography basket catheter in both the femoral and carotid arteries, where the latter served as an atherosclerosis-free control. Temperature measurements with the catheter were performed in five canines in their peripheral and coronary arteries in vivo to assess feasibility and safety as defined by mortality, angiographic dissection or occlusion, arrhythmia, or electrocardiographic evidence of ischemia or infarction.

Results: Figure 1 below shows the results of our initial in vivo animal studies involving the pro-atherosclerotic canines. The average tissue temperature in regions of the carotid arteries did not vary more than ±0.25 °C from the average value of 34.55 °C. Furthermore, the corresponding

blood temperature was essentially identical to that of the surrounding tissue, except for a little less variability. IN the femoral arteries, however, we detected overall higher tissue and blood temperatures. Tissue temperatures ranged from 34.95-35.35 °C with an average of 35.2 °C. On average, this was 0.8 °C hotter than the atherosclerosis-free regions of the carotid arteries. Furthermore, we observed a clearly detectable difference in the femoral blood and tissue temperature of 0.2 °C, an observation consistent with inflamed tissue being hotter than disease-free tissue. Overall, these results suggest viable in vivo applications of our thermo-basket catheter.

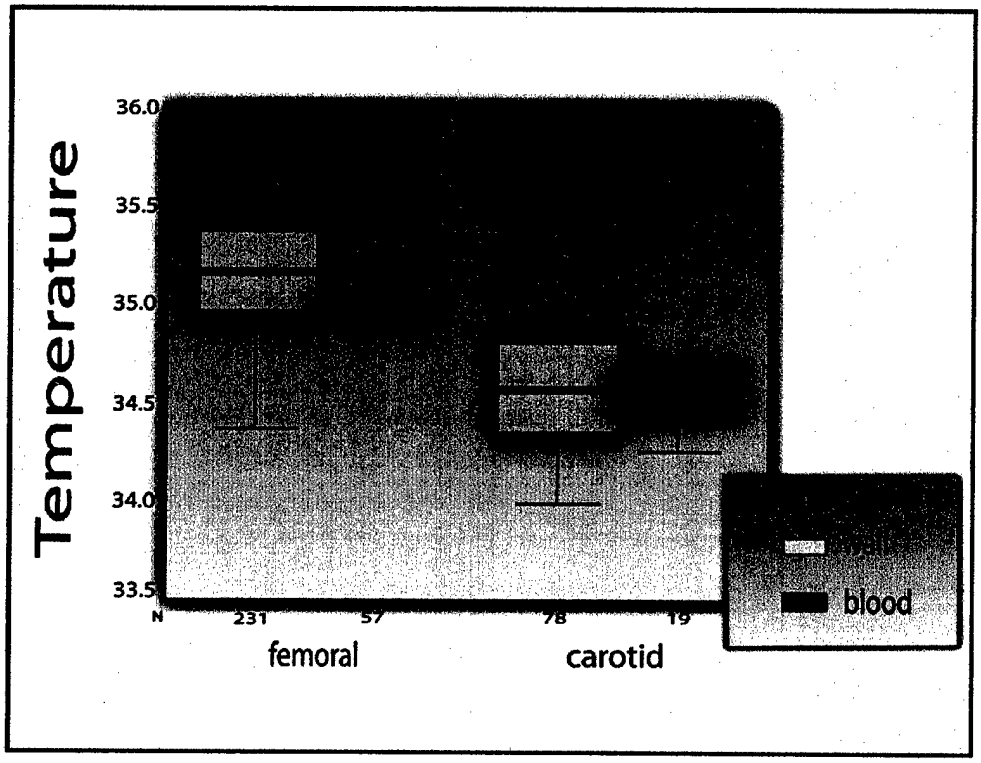

Figure 1. Temperature values of blood and tissue were recorded in two distinct regions (carotid and femoral arteries) of canines in vivo. A four-sensor, thermography basket catheter was used for all measurements. Five animals were utilized for generation of this data.

Project II.E.

Initial Evaluation of a New Axial Flow Pump, Inserted by Minimally Invasive Thoracotomy, to Maintain Cardiac Output in a Porcine Model of Cardiogenic and Hemorrhagic Shock

Investigators: O. Howard Frazier, M.D.
Branislav Radovancevic, M.D.

Project Objectives: The purpose of this project is to investigate a novel approach to reducing mortality and morbidity due to injuries suffered by military personnel in combat zones. Specifically, the objective of this research is to evaluate the use of an implantable mechanical cardiac assist device, in conjunction with standard volume and/or blood replacement, for treatment of hemorrhagic shock resulting from injuries sustained in the combat setting.

Progress Summary: In this series of studies (n=4) the focus of our work was to investigate the humoral and histological components of the mechanism that contribute to the progression of severe hemorrhagic shock to circulatory collapse. Two controls and two experimental studies (LVAD implant) were performed. The control studies were hemorrhaged and resuscitated; the experimental animals were hemorrhaged and resuscitated followed by a LVAD implant. Tissue samples were collected from the lungs, liver and heart at several intervals throughout the study in both groups. These tissue samples were later analyzed in order to determine the intracardiac levels of three pro-inflammatory cytokines.

LVAD/Control Group: Under sterile conditions, a dual chambered polyvinylchloride catheter (Quinton) was placed in the right carotid artery. An oximetric Swan-Ganz thermodilution catheter was inserted into the external jugular and floated into the pulmonary artery for recording pressures, cardiac output, and continuous mixed venous saturation. The catheters were fixed to their respective vessels and tunneled to exit dorsally at the midline. A ventral abdominal incision was made and the spleen removed

after double ligation of all vascular pedicles and the incision site closed in three suture layers. A left thoracotomy at the fifth intercostal space was performed. Baseline tissue sample were then obtained from the left ventricle, the liver and the lungs using s biopsy needle. The Left Coronary Artery (LCA) was isolated and dissected for the placement of a 2.5 mm flow probe.

The instrumentation was connected to the appropriate transducers for a 30 minutes equilibration period. Once the transducers were calibrated, the FIO2 was dropped to 30% and the animals were hemorrhaged to a mean arterial pressure (AoP) of 40 mmHg at which point it was maintained for 30 minutes to simulate a response time. After this 30-minute period, fluid administration was begun (2cc LRS/ 1cc blood loss). After fluid resuscitation an additional set of tissue samples were collected form the liver, lungs and left ventricle. The animals remained under anesthesia and instrumented throughout the remainder of the study and data collected continuously.

LVAD Group: At the end of fluid administration a double pursestring suture was placed on the descending aorta for the insertion of the outflow cannula. Another double pledgeted pursestring suture was placed in the left atria in preparation for the inflow cannula. A small incision was made, the cannula advanced into the left atria and secured with the pursestring suture. The cannulae were primed with heparinized saline and attached to fluid-primed 3/8 tubing and a centrifugal pump. The LVAD was started at a speed of 1,000 RPM and slowly increased to provide maximum support, in one study (b-1400) the LVAD implant was delayed by 2 hours. The animals remained under anesthesia and instrumented throughout the remainder of the study and data collected continuously. If the animal survived to 24 hours or at time of death (if premature), an additional set of tissue samples were collected.

Results:

LVAD GROUP

Surgery Date	Study Type	Animal No.	Animal Wt. (kg)	Survival Time **	Amount of Hemorrhage (ml)
2/12/03	LVAD	B-1400*	115	19	850
5/5/03	LVAD	B-1413	94	24	775
Avg/std			105±15	22±4	813±53

CONTROL GROUP

Surgery Date	Study Type	Animal No.	Animal Wt. (kg)	Survival Time **	Amount of Hemorrhage (ml)
11/25/02	Control	B-1392	127	5	950
5/7/03	Control	B-1414	101	24	882
Avg/std			114±18	15±13	916±48

* This animal had his LVAD implant delayed by two hours.
**Survival time calculated after the end of hemorrhage

The preliminary results of this tissue sample pilot study indicate that there was an increase in intracardiac levels of all three pro-inflammatory cytokines on the control animal and the use of a LVAD in the experimental group blunted the response. This demonstrates that LVAD use may decrease cardiac inflammation as demonstrated by the ability of the LVAD to prevent the increase production of pro-inflammatory cardiac cytokine.

Project II.F.

Physiological Magnetic Resonance Imaging

Investigators: James T. Willerson, M.D.
Silvio H. Litovsky, M.D.
Morteza Naghavi, M.D.

Introduction: Major progress has been made in using MRI to visualize atherosclerotic plaques. MRI may be used to identify atherosclerotic plaques not only in major arteries (aorta and carotid), [1,2] but also in small arteries (coronaries).[3] However, the spatial resolution at which coronary plaques can be studied is limited and largely affected by the anatomical and physiological variables influencing the coronary arteries.[4] Although standard MRI is a powerful tool for detailing plaque morphology (i.e., fibrous cap, lipid core, intraplaque hemorrhage, and calcified areas)[5,6,7,8,9,10] focusing only on the morphological and structural features of atherosclerotic plaques may not be enough. Functional variables, such as endothelial dysfunction and plaque inflammation, are key features that define "vulnerable plaques" (plaques with high likelihood of complications), and techniques are being developed to study these properties in vivo.

Conventional MRI that employs the specific blood pool contrast agent superparamagnetic iron oxide (SPIO) has been proposed to fulfill these diagnostic capabilities. These nanoparticles are more avidly taken up by macrophages than by other cells.[11] The use of SPIO and USPIO (ultra small superparamagnetic iron oxide) nanoparticles as MRI contrast agents for imaging inflammation in atherosclerotic plaque has been studied by Kooi et al.[12] in human carotid arteries and by Ruehm et al[13] and Schmitz et al.[14,15,16] in hypercholesterolemic rabbits. Decreased signal intensity of aortic lesions after injecting SPIO on MRI and MR angiography of the aorta, and histologic evidence of SPIO accumulation in the macrophages of atherosclerotic plaques was reported.

In the present study, we tested the hypothesis that SPIO particles accumulate in atherosclerotic plaques inside macrophages in two animal models, the apoE-deficient mouse and the WHHL (Watanabe hereditable hyperlipidemic) rabbit,

and that SPIO-enhanced MRI can noninvasively identify inflamed atherosclerotic plaques.

MATERIALS AND METHODS:

1. *Studies of Intracellular SPIO Relaxivity*

Peritoneal macrophages were obtained from Balb/C mice by intraperitoneal injection of 0.1 mg of pristine (mineral oil). After 2 days, the mice were sacrificed, the peritoneum opened, and macrophages extracted by peritoneal lavage.

The T2-shortening effect of intracellular SPIO was evaluated at 4 different time points using 4 different concentrations of SPIO. In brief, 10 x 10^5 macrophages were added to each of 4 tubes containing 50, 100, 250, and 500 nmol Fe/ml diluted, respectively, and 2 control tubes containing macrophages but no SPIO and then incubated for varying periods. At several time points (20 min, 1 hour, 6 hours, and 24 hours), 6 tubes (4 containing SPIO at different concentrations and 2 containing controls) were centrifuged at 1000 rpm for 5 minutes, washed with PBS for 5 minutes, and then fixed in paraformaldehyde. This resulted in 24 tubes of macrophages for analysis. Finally, the tubes were stacked and scanned in a 7.1T MRI scanner (Bruker).

2. *Experimental Animals*

For the experiments described below, ApoE-deficient and C57BL/6 mice (10-14 months old), Watanabe hereditary hypercholesterolemic (WHHL) rabbits (2-3 years old), and New Zealand White (NZW) rabbits (1-2 years old) were used. All experimental procedures in these animals were performed in accordance with protocols approved by the Institutional Animal Care and Research Advisory Committee at each participating center.

3. *Pathologic Examination of In Vivo Distribution of SPIO in ApoE-Deficient (Atherosclerotic) vs. Wild-type (Control) Mice*

Seven ApoE-deficient (atherosclerotic) mice and five C57BL/6 (control) mice were injected with SPIO 1 mmol Fe/kg (Feridex, Berlex, New Jersey), via the tail vein. The mice were sacrificed on post-injection days 3 and 5. Tissues

from different organs (including the liver, spleen, kidneys, lung, heart, and bone marrow) and from aortas (including the sinus of Valsalva, ascending, descending, and abdominal regions) were fixed and sent for staining and pathological examination. Stains used were hematoxylin and eosin (H&E), Perls' (iron), and MAC-2 (macrophage). The atherosclerotic aortic walls of the ApoE-deficient mice were compared with the normal aortic walls of the C57BL mice in terms of the number of iron particles per high power field.

4. *Comparison of Pre and Post-SPIO MRI*

ApoE-Deficient vs. Normal Mice

Using a 4.7T MRI scanner (Bruker) with respiratory gating, baseline MRI was performed on 6 ApoE-deficient and 2 wild-type mice (TR = 2500 msec, TE = 12 msec, FOV = 6.6 cm, slice thickness = 2.0 mm, flip angle (orient) = trans, and matrices = 256 x 256 pixels). The mice were then injected with SPIO (1 mmol Fe/kg) IV via the tail vein. Post-contrast MRI was performed on day 5 using the same MRI variables. Pre-contrast (baseline) and post-contrast images of the aorta were compared at the renal level.

5. *Histopathological Examination of In Vivo Distribution of SPIO in Rabbits*

In order to study the distribution of iron in different tissues, 4 WHHL rabbits and 2 NZW rabbits (controls) were injected with SPIO (2 mmol Fe/kg) IV through an ear vein. One WHHL and one NZW rabbit served as untreated controls (i.e., they received no SPIO). Animals were sacrificed on postinjection day 5. Tissues from the aorta as well as liver, spleen, kidneys, and heart were fixed and stained by H&E, and for iron and RAM-11 presence (rabbit anti-macrophage antibody).

6. WHHL vs. NZW Rabbits

In Vivo

Using a 1.5T MRI system (Signa, General Electric) equipped with a conventional extremity coil, baseline MRI of the aortas was done on 4 WHHL and 2 NZW rabbits (T2 gradient echo: TR = 1200 msec, TE = 6 msec, FOV = 16 x 12 cm, matrix size = 256 x 192 pixels; 3-dimensional magnetic resonance

[Ruehm, 2001 #5] angiography with gadolinium-DTPA: TE = 1.3 msec, TR = 5.6 msec). The rabbits were injected with SPIO (2 mmol Fe/kg) IV via an ear vein. Post-contrast MRI was performed on day 5 using the same MRI sequences. The rabbits were anesthetized with isoflurane for the duration of their studies.

Ex Vivo

All rabbits that underwent *in vivo* MRI were sacrificed. Their aortas were excised, isolated, and placed in a gel medium. Both ends of the aorta were clamped and all side branches were occluded. Gadolinium-DTPA was injected inside the lumen. Then, MRI was performed, using the 1.5T scanner used in the *in vivo* experiments. Data on T2 gradient echo and 3D MR angiography sequences were recorded for each specimen.

Results:

1. Intracellular SPIO Relaxivity

A significant relationship was found between cellular SPIO incubation times and T2 shortening and between SPIO doses and T2 shortening ($P<0.05$). The maximum T2 shortening effect was observed to occur at echo time TE = 96 msec and repetition time TR = 3000 msec.

2. In Vivo SPIO Distribution in ApoE-Deficient vs. Wild-Type Mice

Histopathologic studies revealed the accumulation of SPIO particles in the macrophage system in both normal and mice with aortic atherosclerosis, especially in the livers, spleens, and bone marrows. Other tissues, such as the lungs and kidneys also showed some degree of SPIO uptake in macrophages. However, apoE-deficient and wild-type normal mice differed markedly in the extent of SPIO uptake in their aortas and atherosclerotic lesions. Numerous iron particles were seen in aortic atherosclerotic plaques from ApoE-deficient mice, compared with very few in nonatherosclerotic areas of the aortic walls in both normal and ApoE-deficient mice.

3. In Vivo Distribution of SPIO in Rabbits

Histopathologic studies in rabbits also revealed the accumulation of iron in the macrophage system in all tissues, including the arterial wall. Actively inflamed atherosclerotic areas of the aortic wall showed higher uptake of SPIO than did the normal aortic wall and non-inflamed atherosclerotic areas.

4. Comparison of Pre- and Post-SPIO Contrast MRI

ApoE-Deficient vs. Normal Mice

MRI studies showed decreased signal intensity and irregularity in the aortic walls of SPIO-injected ApoE-deficient mice compared with no decrease in signal intensity and no irregularity in SPIO-injected C57BL wild-type (normal) mice. High-resolution images of the aortic wall were obtained at the level of the aortic arches, aortic roots and renal artery level, and renal ostia studies.

WHHL vs. NZW Rabbits (In Vivo)

In vivo MRI studies revealed decreased signal intensity on 3D MR angiography in the aortic walls (data not shown). Because SPIO uptake in the livers, spleens, bone marrows, and other tissues imposed a tissue artifact, changes in T1- and T2-weighted images of the aortas or other arteries could not be appreciated.

WHHL vs. NZW Rabbits (Ex Vivo)

Ex vivo MRI studies were obtained to negate the effects of the tissue artifact mentioned above. As revealed by 3D MR angiography, there were significant luminal irregularities in the aortic walls of SPIO-injected WHHL mice. Also, as shown by T2*- weighted images of the SPIO-injected WHHL mice, SPIO had a negative enhancement effect in the intima and, to some extent, in the medial layer of the atherosclerotic aortic walls.

Discussion: The main findings of this study are: 1) the T2 shortening effect of SPIO is preserved after tissue uptake in vivo, and is concentration and time-dependent; 2) SPIO injected into ApoE-deficient mice accumulates in atherosclerotic plaques; 3) SPIO injected into WHHL rabbits accumulates in certain atherosclerotic lesions

predominantly in superficial foamy cells in the cap region; 4) and SPIO-enhanced MRI in animals with aortic atherosclerosis causes irregular darkening (signal loss) of the aortic wall indicating the presence of active inflammation (iron-loaded macrophages).[17] [18] [1] [19] [3] Others have previously shown that high-resolution imaging of atherosclerotic plaques allows us to detect certain anatomic variables that suggest plaque vulnerability, including the presence of thin fibrous caps and neovascularization.

The use of SPIO as a MRI contrast agent for imaging inflammation in atherosclerotic plaques has been recently studied by Kooi et al [12] in human carotid arteries and by Ruehm et al and Schmitz et al [13] [14] [15] in hypercholesterolemic rabbits. Our studies of SPIO uptake showed that macrophages in cell culture medium avidly take up SPIO and that the uptake of SPIO is dose dependent. Studies of MRI relaxivity revealed that intracellular SPIO retains its superparamagnetic properties to affect tissue relaxation time (especially T2). We also found that alteration in macrophage T2 relaxation changes with the intracellular concentration of SPIO, which itself correlates with the time of exposure to SPIO. The T2 effect is therefore enhanced at higher doses and longer SPIO incubation times.

In the ApoE-deficient mice, the atherosclerotic plaque burden and inflammation were more pronounced in the upper thoracic aorta.[20] Moreover, we found that SPIO was unevenly distributed in the arterial tree. SPIO particles were more frequent in the aortic roots than in distal aortas, rare in the nonatherosclerotic walls, and also found deep inside the plaques in addition to being present in the subendothelium of aortic plaques in rabbits. To our knowledge, this is the first report of MRI with SPIO in the ApoE-deficient mice. Since ApoE-deficient mice do not have a well-developed fibrous cap, we could not locate SPIO particles within the caps of atherosclerotic plaques in these animals. This is in agreement with results of previous studies in ApoE-deficient mice from our group, showing fluorescently labeled macrophages within foam cell atherosclerotic plaques and adhering to the luminal surface of the plaques 48 hours after IV injection.[21] In addition, experiments aimed at quantifying monocyte/macrophage recruitment in atherosclerotic plaques in mice have shown that recruitment varies by stage of atherosclerosis in

these plaques and also by location in the arterial tree [22] [23] [24]

In the MRI studies of aortas, we found changes in mice and rabbits atherosclerotic aortas after SPIO injection. Because of their small sizes and problems with cardiac gating, we could not image the thoracic aorta of mice clearly enough to compare pre- and post-SPIO effects. Therefore, we focused on the changes in the abdominal aortas at the renal level which showed decreased signal intensity in T2-weighted images. This effect was not seen in control animals.

Limitations: Our present study represents the beginning of a series of experiments aimed at developing plaque-targeted SPIO as an MRI contrast agent to identify vulnerable atherosclerotic plaques. The study has led to more questions than answers. For instance, we do not know the major avenue of SPIO entry into plaques. Are SPIO particles preferentially taken up by circulating monocytes, or do they enter freely into plaques where they are then taken up by active macrophages present in the plaque? We do not know how long SPIO particles, once taken up, remain in plaques. We do not know the optimal particle size or dose. We do not know what, if any, dose-dependent side effects of SPIO occur. Moreover, even though we have shown a possible correlation between vulnerability (i.e., plaque inflammation/macrophage infiltration) and SPIO accumulation, our study was not designed to look for comprehensive evidence of vulnerability (i.e., vascular events due to plaque rupture and thrombus formation). Because of intrinsic limitations of the animal models, we did not correlate macrophage infiltration within the atherosclerotic lesions with other criteria of plaque vulnerability, such as cap thickness, lipid core size, and intraplaque hemorrhage. There is also the problem of limited image resolution and signal-to-noise ratio (SNR) with contemporary MRI. Poor spatial resolution also limits the power to correlate SPIO accumulation in atherosclerotic plaques with decreased signal intensity on MRI.

Conclusions: SPIO-enhanced MRI was studied as a noninvasive means to detect macrophage infiltration in atherosclerotic plaques in the aortic walls of ApoE-deficient mice and WHHL rabbits. Our findings suggest that SPIO-enhanced MRI may

have significant potential for diagnosis of vulnerable plaques.

References:

1. Yuan C, Petty C, O'Brien KD, Hatsukami TS, Eary JF, Brown BG. In vitro and in situ magnetic resonance imaging signal features of atherosclerotic plaque-associated lipids. *Arterioscler Thromb Vasc Biol*. 1997;17:1496-503.

2. Schmitz SA, Taupitz M, Wagner S, Wolf KJ, Beyersdorff D, Hamm B. Magnetic resonance imaging of atherosclerotic plaques using superparamagnetic iron oxide particles. *J Magn Reson Imaging*. 2001;14:355-61.

3. Fayad ZA, Fuster V, Fallon JT, Jayasundera T, Worthley SG, Helft G, Aguinaldo JG, Badimon JJ, Sharma SK. Noninvasive in vivo human coronary artery lumen and wall imaging using black-blood magnetic resonance imaging. *Circulation*. 2000;102:506-10.

4. Botnar RM, Stuber M, Kissinger KV, Kim WY, Spuentrup E, Manning WJ. Noninvasive coronary vessel wall and plaque imaging with magnetic resonance imaging. *Circulation*. 2000;102:2582-7.

5. Fayad ZA, Fallon JT, Shinnar M, Wehrli S, Dansky HM, Poon M, Badimon JJ, Charlton SA, Fisher EA, Breslow JL, Fuster V. Noninvasive In vivo high-resolution magnetic resonance imaging of atherosclerotic lesions in genetically engineered mice. *Circulation*. 1998;98:1541-7.

6. Choudhury RP, Aguinaldo JG, Rong JX, Kulak JL, Kulak AR, Reis ED, Fallon JT, Fuster V, Fisher EA, Fayad ZA. Atherosclerotic lesions in genetically modified mice quantified in vivo by non-invasive high-resolution magnetic resonance microscopy. *Atherosclerosis*. 2002;162:315-21.

7. Braun A, Trigatti BL, Post MJ, Sato K, Simons M, Edelberg JM, Rosenberg RD, Schrenzel M, Krieger M. Loss of SR-BI expression leads to the early onset of occlusive atherosclerotic coronary artery disease, spontaneous myocardial infarctions, severe cardiac dysfunction, and premature death in apolipoprotein E-deficient mice. *Circ Res*. 2002;90:270-6.

8. Helft G, Worthley SG, Fuster V, Fayad ZA, Zaman AG, Corti R, Fallon JT, Badimon JJ. Progression and regression of atherosclerotic lesions: monitoring with serial noninvasive magnetic resonance imaging. *Circulation*. 2002;105:993-8.

9. Helft G, Worthley SG, Fuster V, Zaman AG, Schechter C, Osende JI, Rodriguez OJ, Fayad ZA, Fallon JT, Badimon JJ. Atherosclerotic aortic component quantification by noninvasive magnetic resonance imaging: an in vivo study in rabbits. *J Am Coll Cardiol*. 2001;37:1149-54.

10. Zimmermann-Paul GG, Quick HH, Vogt P, von Schulthess GK, Kling D, Debatin JF. High-resolution intravascular magnetic resonance imaging: monitoring of plaque formation in heritable hyperlipidemic rabbits. *Circulation*. 1999;99:1054-61.

11. Pouliquen D, Le Jeune JJ, Perdrisot R, Ermias A, Jallet P. Iron oxide nanoparticles for use as an MRI contrast agent: pharmacokinetics and metabolism. *Magn Reson Imaging*. 1991;9:275-83.

12. Kooi ME, Cappendijk VC, Cleutjens KB, Kessels AG, Kitslaar PJ, Borgers M, Frederik PM, Daemen MJ, van Engelshoven JM. Accumulation of ultrasmall superparamagnetic particles of iron oxide in human atherosclerotic plaques can be detected by in vivo magnetic resonance imaging. *Circulation*. 2003;107:2453-8.

13. Ruehm SG, Corot C, Vogt P, Kolb S, Debatin JF. Magnetic resonance imaging of atherosclerotic plaque with ultrasmall superparamagnetic particles of iron oxide in hyperlipidemic rabbits. *Circulation*. 2001;103:415-22.

14. Schmitz SA, Winterhalter S, Schiffler S, Gust R, Wagner S, Kresse M, Coupland SE, Semmler W, Wolf KJ. USPIO-enhanced direct MR imaging of thrombus: preclinical evaluation in rabbits. *Radiology*. 2001;221:237-43.

15. Schmitz SA, Coupland SE, Gust R, Winterhalter S, Wagner S, Kresse M, Semmler W, Wolf KJ. Superparamagnetic iron oxide-enhanced MRI of atherosclerotic plaques in Watanabe hereditable hyperlipidemic rabbits. *Invest Radiol*. 2000;35:460-71.

16. Schmitz SA, Taupitz M, Wagner S, Coupland SE, Gust R, Nikolova A, Wolf KJ. Iron-oxide-enhanced magnetic resonance imaging of atherosclerotic plaques: postmortem analysis of accuracy, inter-observer agreement, and pitfalls. *Invest Radiol*. 2002;37:405-11.

17. Toussaint JF, LaMuraglia GM, Southern JF, Fuster V, Kantor HL. Magnetic resonance images lipid, fibrous, calcified, hemorrhagic, and thrombotic components of human atherosclerosis in vivo. *Circulation*. 1996;94:932-8.

18. Toussaint JF, Southern JF, Kantor HL, Jang IK, Fuster V. Behavior of atherosclerotic plaque components after in vitro angioplasty and atherectomy studied by high field MR imaging. *Magn Reson Imaging*. 1998;16:175-83.

19. Yuan C, Zhang SX, Polissar NL, Echelard D, Ortiz G, Davis JW, Ellington E, Ferguson MS, Hatsukami TS. Identification of fibrous cap rupture with magnetic resonance imaging is highly associated with recent transient ischemic attack or stroke. *Circulation*. 2002;105:181-5.

20. Nakashima Y, Plump AS, Raines EW, Breslow JL, Ross R. ApoE-deficient mice develop lesions of all phases of atherosclerosis throughout the arterial tree. *Arterioscler Thromb*. 1994;14:133-40.

21. Patel SS, Thiagarajan R, Willerson JT, Yeh ET. Inhibition of alpha4 integrin and ICAM-1 markedly attenuate macrophage homing to atherosclerotic plaques in ApoE-deficient mice. *Circulation*. 1998;97:75-81.

22. Steinberg D, Khoo JC, Glass CK, Palinski W, Almazan F. A new approach to determining the rates of recruitment of circulating leukocytes into tissues: application to the measurement of leukocyte recruitment into atherosclerotic lesions. *Proc Natl Acad Sci U S A*. 1997;94:4040-4.

23. Kim CJ, Khoo JC, Gillotte-Taylor K, Li A, Palinski W, Glass CK, Steinberg D. Polymerase chain reaction-based method for quantifying recruitment of monocytes to mouse atherosclerotic lesions in vivo: enhancement by tumor necrosis factor-alpha and interleukin-1 beta. *Arterioscler Thromb Vasc Biol*. 2000;20:1976-82.

24. Litovsky S, Madjid M, Zarrabi A, Casscells SW, Willerson JT, Naghavi M. Superparamagnetic iron oxide-based method for quantifying recruitment of Monocytes to mouse atherosclerotic lesions in vivo: enhancement by tissue necrosis factor-alpha, interleukin-1beta, and interferon-gamma. *Circulation*. 2003;107:1545-9.

Project III.A.

Induction of Chemokine Expression in Endothelial Cells by C-Reactive Protein

Investigator: Edward T.H. Yeh, M.D.

Introduction: Inflammation is now known to be a major player in the development of atherosclerosis and its subsequent events, such as acute coronary syndrome. C-Reactive Protein (CRP) has been shown to be an excellent marker of inflammation that also predicts the risk of heart attack in apparently healthy men and women. We have shown that CRP can directly activate human coronary endothelial cells. Thus, CRP is not only a marker, but also a culprit in setting up a chain of events that eventually leads to heart attack. CRP, named for its capacity to binds to the C-polysaccharide of *Streptococcus pneumoniae*, was the first acute-phase protein to be described (10).

CRP, as other acute phase proteins, is synthesized by the liver in response to microbial infection, tissue injury, and autoimmune disorders. It had been shown that IL-1β and IL-6 strongly induced the expression of CRP in human hepatocytes and in hepatoma cells. Recently, human neuronal cells were found to produce CRP in Alzheimer's disease. In addition, renal cortical tubular epithelial cells were shown to produce CRP following inflammatory stimuli. Interestingly, CRP has also been found in human atherosclerotic plaques, which could be due to indirect deposit from circulating cells or direct production by cells in the arterial wall.

Research accomplishments: Human coronary artery smooth muscle cells (HCASMCs) and human umbilical vein endothelial cells (HUVECs) were incubated with IL-1□, IL-6, their combination, TNF-α, or LPS at different concentrations. The supernatants were concentrated and analyzed by a high sensitivity ELISA specific for human CRP. RNA was extracted from the HCASMCs for RT-PCR using specific primers for the CRP. Maximal CRP production was observed in HCASMCs after 48 hours of incubation with the combination of 25 ng/ml of IL-1□ and 10 ng/ml of IL-6,

while incubation with IL-1□ or IL-6 alone only modestly induced CRP (Fig. A). Incubation with TNF-α (50 ng/ml) or with LPS (1000 EU/ml) resulted in an increase in CRP production comparable to the IL-1□ and IL-6 combination (Fig. B). The induction of CRP in HCASMCs was independently confirmed by RT-PCR comparing the relative CRP mRNA levels.

Conclusions: These results identified for the first time that HCASMCs, but not HUVECs, can produce CRP in response to inflammatory cytokines.

Publications:

1. Calabro, P.; Willerson, J.T.; Yeh, E.T.H. Inflammatory cytokines stimulated C-reactive protein production by human coronary artery smooth muscle cells, *Circulation*, In Press.

Project III.B.

Nitrotyrosine Formation, Metabolism and Function: Functions of Nitric Oxide and Nitrotyrosine in Shock, Sepsis, and Inflammation

Investigator: Ferid Murad, M.D., Ph.D.

Introduction: The biological effects of nitric oxide may be due to increased cyclic GMP synthesis by guanylyl cyclase or by cyclic GMP-independent pathways. With regard to the latter, one of the important effects of nitric oxide is the interaction with superoxide anion to form peroxynitrite. Peroxynitrite is very reactive and can modify proteins, DNA and lipids. One of its effects is to form nitrotyrosine with tyrosine residues in proteins or with free tyrosine. Our laboratory is examining the proteins that may contain nitrotyrosine in order to identify these proteins and determine their function. Our hypothesis is that protein nitration is a common mechanism by which inflammation caused dysfunctional changes in cells. Once formed, nitrated proteins may exacerbate the pathogenic process and play a role in the connection between inflammation and following complications.

Results: In order to induce inflammatory processes and increase peroxynitrite and nitrotyrosine formation we have administered LPS (endotoxin) or proinflammatory cytokines such as IFN-γ, IL-1, or TNF-α to cell cultures or intact animals (rats). We have also induced diabetes in rats with the administration of streptozotocin, a well-known model to produce diabetes. Another model of gastrointestinal inflammation has been the oral administration to rats and mice of the parasite, *Trichinella spiralis*.

Tissue samples are homogenized and fractions are applied to 1-D and/or 2-D PAGE for the separation of proteins. We use commercial nitrotyrosine antibodies and those that we have prepared for nitrotyrosine immuno-histochemistry and/or Western immunoblots. Tissue sections have also been examined by immunohistochemical techniques for nitrotyrosine. Nitrated proteins are further identified by matrix-assisted laser desorption ionization/time-of-flight

mass spectrometric analysis (MALDI-TOF) of in-gel tryptic digest of nitrotyrosine immunopositive bands.

We have screened different organs for nitrated proteins. Many nitrated proteins were identified and some of them were functionally characterized. The data are presented in several publications (3, 8, 11, 13-20, 25). Here, we want to underline some general issues, which became apparent from our studies.

- Protein tyrosine nitration is a residue, protein and tissue selective process. Certain proteins can be preferential targets for nitration. This selectivity may depend on the composition and structure of a given target, its intracellular concentration, localization and interaction with other molecules.
- Studies on functional consequences of nitration provide evidences that nitration adversely affects properties of proteins.
- Specific proteins nitrated *in vivo* in the different models of inflammation are involved in major cell functions, such as signal transduction, energy production, antioxidant defense, and apoptosis.

Taken together, our results support the view that protein tyrosine nitration may be an important process that participates in cellular regulation under normal and pathological conditions. Out of many proteins found nitrated, for further detailed functional studies, we have selected two proteins, which functions have closest relation to studies pursuit in the lab. This is L-type Ca^{2+}-channel and protein kinase G. Both proteins are important for contraction/relaxation of smooth muscles.

This lab has long-standing interest in $^{\bullet}NO$ regulated smooth muscle relaxation. Protein tyrosine nitration is a portion of $^{\bullet}NO$ biology. Recently, we have published data (20) that demonstrate nitration of α1C subunit of L-type Ca^{2+} channel in the intestinal smooth muscle tissue, jejunum, from *Trichinella spiralis* treated rats. *Trichinella spiralis* are one host helminthes that cause inflammation and nitrotyrosine formation in intestine. Contraction experiments with strips of longitudinal muscle from control and *Trichinella spiralis* infected jejunum indicated a marked delay in the onset and a decrease in the velocity of

the phasic phase of a carbachol-induced contraction. The potassium-induced contraction also was markedly inhibited. To our knowledge, this is the first observation that may link changes in contractile function of smooth muscle and the nitration of specific protein involved in contraction. Identification of other nitrated proteins and detailed studies on their functions are required to assess the role of protein nitration in smooth muscle pathogenesis.

Apart from biological significance of protein nitration, the mechanism(s) of tyrosine nitration *in vivo* is also a subject of our interest. Besides peroxynitrite, additional mechanisms may contribute in the protein tyrosine nitration *in vivo*. Pro-oxidant effects of free and chelated iron have attracted our attention. For the first time, the systematic analysis of nitrotyrosine formation by either heme or free iron was performed. We found that free iron/heme cause protein nitration (18). This mechanism of protein nitration may be especially relevant to iron and heme enriched tissues, such as heart and skeletal muscle.

Conclusions: It is evident that inflammatory diseases are associated with progressive changes in the production of reactive oxygen and nitrogen species and with increased formation of tyrosine nitrated proteins. The nitration of protein tyrosine residues has been used as a marker of oxidative stress in inflammation. Understanding how protein nitration occurs and what are the functional consequences of nitration will offer new options for design of antioxidant therapy in the treatment of inflammatory diseases. The current study represents a systematic effort to investigate the biological role of protein tyrosine nitration.

Publications:

1. Martin, E., Davis, K., Bian, K., Lee, Y.C., and Murad, F. Cellular signaling with NO and cyclic GMP. **Seminars in Perinatology** 24, 2-6, 2000.

2. Kildsgaard, J., Hollmann, T., Matthews, K., Bian, K., Murad, F. and Wetsel, R. Increased susceptability to endotoxin shock in complement C3a receptor deficient mice indicates an anti-inflammatory role for the C3a anaphylatoxin. **Journal of Immunology.** 165, 5406-5409, 2000.

3. Ishii, N., Patel, K.P., Lane, P.H., Taylor, T., Bian, K., Murad, F., Pollock, J.S., and Carmines, P.K. Nitric oxide synthesis and oxidative stress in the renal cortex of rats with diabetes mellitus. **J. Amer. Soc. Nephrology** 12, 1630-1639, 2001.

4. Mendes, R.V., Martins, A.R., de Nucci, G., Murad, F., and Soares, F.A. Expression of nitric oxide synthase isoforms and nitrotyrosine immunoreactivity by B-cell non-Hodgkin's lymphomas and multiple myeloma. **Histopathology** 39, 172-178, 2001.

5. Bian, K., Harari, Y., Zhong, M., Lai, M., Castro, G., Weisbrodt, N., and Murad, F. Down regulation of inducible nitric oxide synthase during parasite-induced gut inflammation. A path to identify a selective NOS-2 inhibitor. **Molecular Pharmacology** 59, 939-947, 2001.

6. Mailman, D., Guntuku, S., Bhuiyan, B. and Murad, F. Sites of LPS-induced nitric oxide production in the anesthetized rat. **Nitric Oxide: Biology and Chemistry 5,** 243-251, 2001.

7. Davis, K., Martin, E., Turko, I. and Murad, F. Novel effects of nitric oxide, **Annual Review of Pharmacology and Toxicology**. 41, pp. 203-236, 2001.

8. Marcondes, S., Turko, I., and Murad, F. Nitration of succinyl Co-A-axoacid transferase decreases enzyme activity with endotoxin administration. **Proc. Nat. Acad. Sci.** 98, 7146-7151, 2001.

9. Seminara, A.R., Krumenacker, J.S., and Murad, F. Signal transduction with nitric oxide, guanylyl cyclase and cyclic GMP. In Proc. of the NATO meeting on Nitric Oxide, Sicily, NATO Science Series 317, 5-22, 2001.

10. Hanafy, K., Krumenacker, J. and Murad, F. Nitric oxide and cyclic GMP cellular signaling. Proceedings of the Vascular Biology Conference, Cracow, Poland, Medical Science Monitor 7 (4), 801-819, 2001.

11. Turko, I., Marcondes, S., and Murad, F. Diabetes-associated nitration of tyrosine and inactivation of succinyl-CoA:3-oxoacid CoA transferase. **Physiol. Amer. J. Physiol., Heart Circ** 281, H2289-H2294, 2001.

12. Bian, K., Zhong, M., Harari, Y., Weisbrodt, N., and Murad, F. Down regulation of inducible nitric oxide synthase by an IL4Rα/Stat6-dependent and T-cell independent pathway during parasite-induced gut inflammation. **Mol Pharmacol.** 59(4):939-47, 2001.

13. Bian, K., and Murad, F. Diversity of endotoxin-induced nitrotyrosine formation in macrophage - endothelium rich tissue. **Free Radical Biology and Medicine** 31(4):421-429, 2001.

14. Turko, I., and Murad, F. Protein nitration in cardiovascular diseases. **Pharmacological Reviews** 54, 619-634, 2002.

15. Adewuya, O., Irie, Y., Bian, K., Onigu-Otite, E., and Murad, F. Mechanism of vasculitis and aneurysms in a mouse model of Kawasaki Diseased: Role of nitric oxide. **Nitric Oxide: Biology and Chemistry.** 8, 15-25, 2003.

16. Murad, F. The excitement and rewards of research with our discovery of some of the biological effects of nitric oxide. **Circulation Research** 92:339-41, 2003.

17. Irie, Y., Saeki, M., Kamisaki, Y., Martin, E., and Murad, F. Histone H1.2 is a substrate for denitrase, an activity that reduces nitrotyrosine immunoreactivity in protein. **Proc. Nat. Acad. Sci.** 100, 5634-5639, 2003.

18. Bian, K., Gao, Z., Weisbrodt, N., and Murad, F. The nature of heme/iron-induced protein tyrosine nitration. **Proc. Nat. Acad. Sci.** 100, 5712-5717, 2003.

19. Turko, I., Li, L., Aulak, K., Stuehr, D., Chang, R., and Murad, F. Protein tyrosine nitration in the mitochondria from diabetic mouse heart. **J. Biol. Chem.** 278, 33972-33977, 2003.

20. Bian, F., and Murad, F. Nitric oxide (NO) - biogeneration, regulation, and relevance to human diseases. **Frontiers in Bioscience** 8, 264-278, 2003.

21. Turko, I., and Murad, F. Quantitative protein profiling in heart mitochondria from diabetic rats. **J. Biol. Chem.** 278, 35844-35849, 2003.

22. Sullivan, J.C., Loomis, E.D., Collins, M., Murad, F., Imig, J.D., Inscho, E.W., and Pollock, J.S. Effect of age on vascular reactivity and oxidative stress in mesenteric arteries from male and female rats. AJP: Regulatory. **Amer. J. Physiol.** (Submitted),

23. Deng, W., Li, C., Liao, L., Zhao, Z., Ge, W., You, S., Deng, H., Zhao, R., and Murad, F. Bone marrow-derived cells give rise to skin cells and regenerate skin tissue. **Dermatology** (Submitted).

24. Bian, K., Harari, Y., Weisbrodt, N., and Murad, F. Helminth regulation of host IL-4Rα/Stat6 signaling:

mechanism underlying NOS-2 inhibition by *Trichinella spiralis*" . **J. of Immunology.** (Submitted).

25. Rossini, L., Martin, E., Zhong, M., and Murad, F. Nitration of inducible nitric oxide synthase tyrosine residues in RAW 264.7 macrophages. **Pharmacological Res.** (Submitted).

Project III.C.

Genes Regulating Wound Healing and Susceptibility to Oxidative Injury

Investigators: Yong-Jian Geng, M.D., Ph.D.

Specific Aim: In this study, we will use microarray techniques to screen genes which can regulate DNA repair and wound healing as well as cell susceptibility to oxidative injury.

Materials and Methods:

cDNA Array Assays: Total RNA was isolated from five aortas of either Apo E-deficient mice or wild type mice using a total RNA isolation kit (Ambion, Austin, TX). Poly A+ mRNA purified from 60 μg of total RNA was reverse transcribed to prepare ^{32}p-labeled cDNA probe. The cDNA probe was purified with CHROMA SPIN column and then hybridized to the Atlas Array membranes (Clontech, Palo Alto, CA) overnight. The membranes were processed as described by the company.

Sequence Analysis: Sequence similarity search was performed with PW29 (gi699609) using BLASTN at NCBI.

Cell Culture And Viability: Human embryonic kidney cell line T-Rex 293 was purchased from Invitrogen (Carlsbad, CA) and grown in a CO_2 incubator at 37°C in DMEM containing 10 % FBS. Mouse vascular smooth muscle cells (mVSMCs) were isolated from aortas by explantation after removal of adventitial connective tissue and endothelium, maintained in DMEM with 10 % FBS, and stored in liquid nitrogen tank until used. Cell viability and apoptosis were determined by staining with acridine orange/ehtidium bromide or with FITC-Annexin V.

Results: PW29 was initially isolated using antibodies raised against pokeweed agglutinin-binding proteins and identified as a calcium-binding protein in nuclei. Cleavage of PW29 during cell division is necessary for coordinated separation of sister chromatids at the onset of anaphase. PW29 is also cleaved during apoptosis and the carboxy

terminal portion is translocated into the cytoplasm. Overexpression of either PW29-GFP fusion protein or the C-terminal portion induces apoptosis in different cell lines. cDNA array assays performed in our laboratory identified PW29 as one of the highly expressed in the aortas of Apo E-deficient mice compared to those of wild type c57BL/6J mice. Sequence analysis revealed the 5'-untranslated region (5'-UTR)of PW29 mRNA is complementary to the coding sequence of ribosomal protein s11(rps11) mRNA.

Since the RNA interference has been known to play an important role for silencing gene expression at different levels of transcription and translation, we studied expression of the PW29 and rps11 mRNAs for their coordinated regulation during apoptosis. In particular, the 5'-UTR of PW29 was overexpressed from a CMV promoter controlled by tetracycline in both T-Rex293 cells and mVSMCs to study its effects on cell proliferation and apoptosis. Our studies showed the following results: 1. Expression of PW29 mRNA is enhanced in the atherosclerotic aortas of Apo E-deficient mice (Fig. 1). 2. The 5'-UTR of PW29 mRNA is complementary to the ribosomal protein S11 mRNA. 3. Both PW29 and RPS 11 mRNAs are cosuppressed in cultured mVSMCs during apoptosis induced by 7-ketocholesterol (Fig. 2). 4. T-Rex 293 cells stably transfected with a cDNA of the 5'-UTR (PW29) were not different in cell proliferation from the untransfected cells.

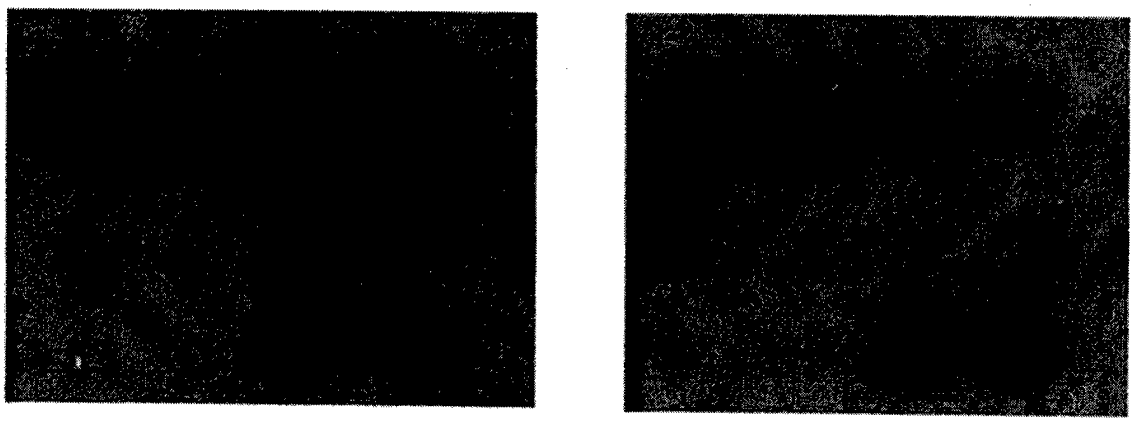

Figure 1. Enhanced Expression of PW29 in the aortas of ApoE-deficient mice (left panel, arrow) compared to wild-type control mice (right panel, arrow).

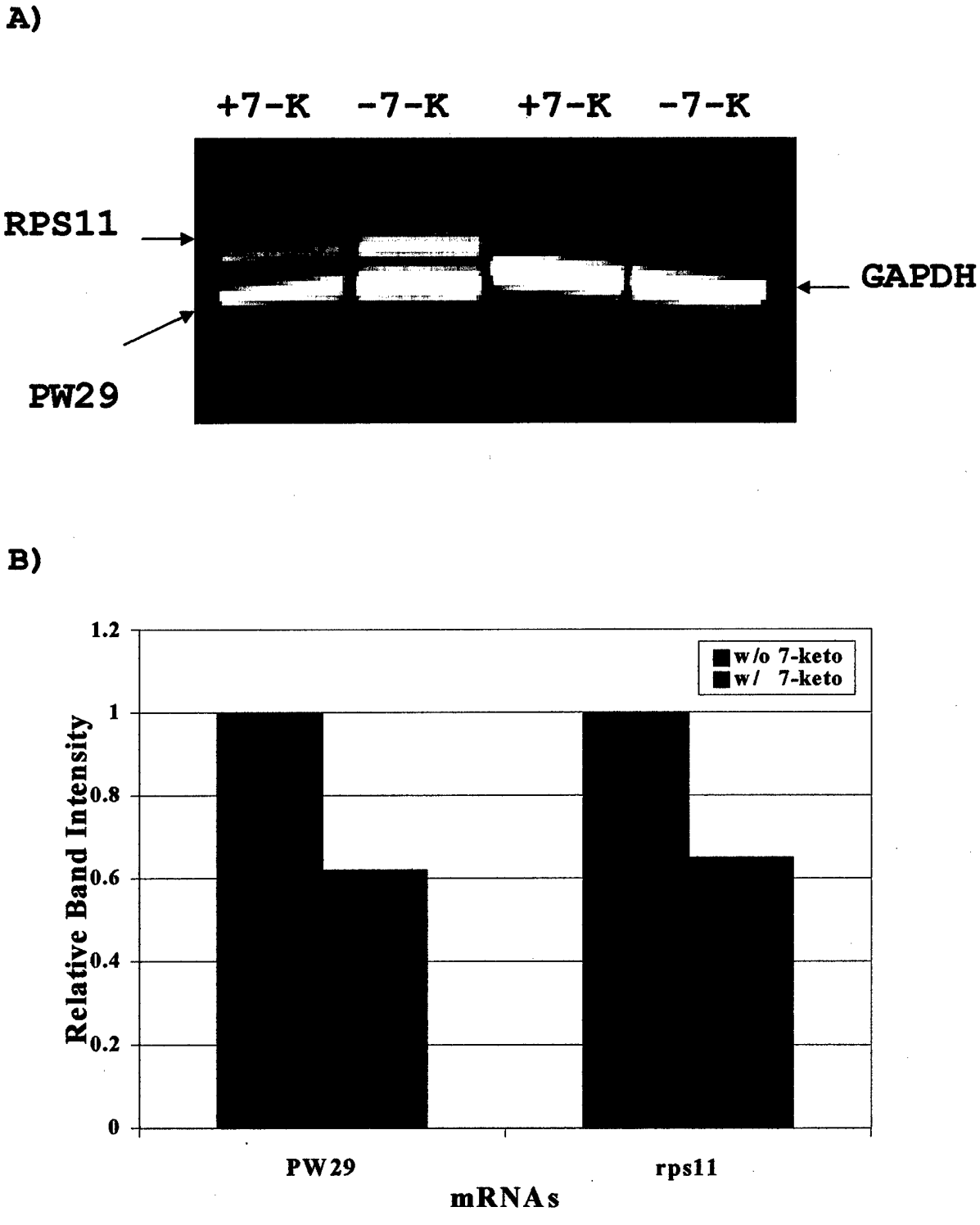

Figure 2. Expression of PW29 and rps11 mRNA during apoptosis induced by 7-ketocholesterol